REPORT DOCUMENTATION PAGE

Form Approved
OMB NO. 0704-0188

1. AGENCY USE ONLY (Leave Blank)	2. REPORT DATE	3. REPORT TYPE AND DATES COVERED
	15 May 2003	Final Report (1 June 1999-31 May 2002)

4. TITLE AND SUBTITLE
High Resolution Core-Level Photoemission Spectroscopy of Semiconductor-Oxide and Metal-Metal Interfaces

5. FUNDING NUMBERS
DAAD 19-99-1-0257

6. AUTHOR(S)
John E. (Jack) Rowe PI/PD and Theodore E. Madey Co-PI/PD

7. PERFORMING ORGANIZATION NAME(S) AND ADDRESS(ES)
Rutgers, The State University of New Jersey
Office of Research and Sponsored Programs
3 Rutgers Plaza, New Brunswick, NJ 08901

8. PERFORMING ORGANIZATION REPORT NUMBER
2002-1

9. SPONSORING / MONITORING AGENCY NAME(S) AND ADDRESS(ES)
U. S. Army Research Office
P.O. Box 12211
Research Triangle Park, NC 27709-2211

10. SPONSORING / MONITORING AGENCY REPORT NUMBER
40167.1-PH-SR

11. SUPPLEMENTARY NOTES
The views, opinions and/or findings contained in this report are those of the author(s) and should not be construed as an official Department of the Army position, policy or decision, unless so designated by other documentation.

12 a. DISTRIBUTION / AVAILABILITY STATEMENT
Approved for public release; distribution unlimited.

12 b. DISTRIBUTION CODE

13. ABSTRACT (Maximum 200 words)

The focus of this project is the characterization of two types of interfaces of technological importance: SiO_2/Si interfaces relevant to ultrathin gate oxides used for next-generation semiconductor electronics, and bimetallic interfaces (ultrathin films of metals on other metals) that have potential catalytic applications. The main tool is high resolution soft-x-ray photoemission spectroscopy (SXPS) using synchrotron radiation at the National Synchrotron Light Source (NSLS). Device-grade films of silicon dioxide and silicon nitride have been grown on Si substrates and new insights into the control of interface electronic state density are found. In addition, SXPS has provided new results on the stability of transition metal films on tungsten substrates: monolayers of Pt, Pd, Ir, Rh are thermally stable, but multilayer films of the same metals form surface alloys.

14. SUBJECT TERMS

15. NUMBER OF PAGES
3+Appendices

16. PRICE CODE

17. SECURITY CLASSIFICATION OR REPORT	18. SECURITY CLASSIFICATION ON THIS PAGE	19. SECURITY CLASSIFICATION OF ABSTRACT	20. LIMITATION OF ABSTRACT
UNCLASSIFIED	UNCLASSIFIED	UNCLASSIFIED	UL

REPORT DOCUMENTATION PAGE (SF298)
(Continuation Sheet)

Final Report
"High Resolution Core-Level Photoemission Spectroscopy of Semiconductor-Oxide and Metal-Metal Interfaces"
1 June 1999 – 31 May 2002
DAAD-99-1-0257

Jack E. Rowe, PI/PD
Theodore E. Madey*, Co-PI/PD
Dept. of Physics and Astronomy
Rutgers, The State University of New Jersey
136 Frelinghuysen Road
Piscataway, NJ 08854
Email: madey@physics.rutgers.edu

*author for Correspondence

1. Statement of Problem and Summary

The focus of this project is the characterization of two types of interfaces of technological importance: SiO_2/Si interfaces relevant to ultrathin gate oxides used for next-generation semiconductor electronics, and bimetallic interfaces (ultrathin films of metals on other metals) that have potential catalytic applications. The main tool is high resolution soft-x-ray photoemission spectroscopy (SXPS) using synchrotron radiation at the National Synchrotron Light Source (NSLS). Device-grade films of silicon dioxide and silicon nitride have been grown on Si substrates and new insights into the control of interface electronic state density are found. In addition, SXPS has provided new results on the stability of transition metal films on tungsten substrates: monolayers of Pt, Pd, Ir, Rh are thermally stable, but multilayer films of the same metals form surface alloys.

2. List of papers published or submitted under ARO sponsorship during this contract.

A. Published in peer-reviewed journals (selected reprints attached as appendices)

(a) "Band offsets for ultrathin SiO_2 and Si_3N_4 films on Si(111) and Si (100) from photoemission spectroscopy.", J.W. Keister, J.E. Rowe, J.J. Kolodziej, H. Niimi, T.E. Madey and G. Lucovsky. J. Vac. Sci. Technol. B17 (1999) 1831-1835.

(b) "Structure of ultrathin SiO_2/Si(111) interfaces studied by photoelectron spectroscopy", J.W. Keister, J.E. Rowe, J.J. Kolodziej, H. Niimi, H.-S. Tao, T.E. Madey and G. Lucovsky. .J. Vac. Sci. Technol. A17 (1999) 1250-1257.

(c) "Photoemission spectroscopy of platinum overlayers on silicon dioxide films", J.W. Keister, J.E. Rowe, J.J. Kolodziej and T.E. Madey. J. Vac. Sci. Technol. B18 (2000) 2174-2178.

(d) "Photoelectron spectroscopy studies of growth, alloying, and segregation for transition-metal films on tungsten (211)", J.J. Kolodziej, T.E. Madey, J.W. Keister and J.E. Rowe. PRB 62 (2000) 5150-5162.

(e) "Photoelectron spectroscopy studies of growth, thermal stability, and alloying for transition metal-tungsten (111) bimetallic systems", J.J. Kolodziej, T.E. Madey, J.W. Keister and J.E. Rowe. PRB 65 (2002) 075413-1-13

(f) "Nanoscale surface chemistry", T. E. Madey, K. Pelhos, Q. Wu, R. Barnes, I. Ermanoski, W. Chen, J. J. Kolodziej, and J. E. Rowe. Proc. Nat. Acad. Sci. 99 (2002) 6503-6508.

B. Submitted but not yet published.
   (a) "Ultrathin Pd and Pt Films on W(211), J. Block, J.J. Kolodzeij, J.E. Rowe, T.E. Madey, and E. Schröder (to be published in Thin Solid Films)
   (b) "A High Resolution Photoemission Study of Surface Core-Level Shifts (SCLS) in Clean and Oxygen Covered Ir(210) Surfaces", M.J. Gladys, I. Ermanoski, G. Jackson, J.S. Quinton, J.E. Rowe and T.E. Madey (to be published in J. Electron Spectroscopy)

3. List of Scientific Personnel

   Dr. Theodore E. Madey
   Dr. John E. (Jack) Rowe
   Dr. Jacek Kolodziej
   Dr. Gavin Jackson
   Mr. Ivan Ermanoski
   Mr. Michael Gladys
   Dr. Jamie Quinton
   Dr. Jeff Keister
   Dr. Marc Ulrich

4. Appendices: Selected reprints of published papers.

Band offsets for ultrathin SiO_2 and Si_3N_4 films on Si(111) and Si(100) from photoemission spectroscopy

J. W. Keister[a)]
Department of Physics, North Carolina State University, Raleigh, North Carolina 27695-8202 and National Research Council Postdoctoral Associate at the Army Research Office, Research Triangle Park, North Carolina 27709-2211

J. E. Rowe
Department of Physics, North Carolina State University, Raleigh, North Carolina 27695-8202, Physics and Astronomy Department and Laboratory for Surface Modification, Rutgers University, Piscataway, New Jersey 08855-0849, and Physics Division, Army Research Office, Research Triangle Park, North Carolina 27709-2211

J. J. Kolodziej
Physics and Astronomy Department and Laboratory for Surface Modification, Rutgers University, Piscataway, New Jersey 08855-0849

H. Niimi
Department of Materials Science and Engineering, North Carolina State University, Raleigh, North Carolina 27695-8202

T. E. Madey
Physics and Astronomy Department and Laboratory for Surface Modification, Rutgers University, Piscataway, New Jersey 08855-0899

G. Lucovsky
Department of Physics, North Carolina State University, Raleigh, North Carolina 27695-8202

(Received 26 March 1999; accepted 27 May 1999)

High resolution soft x-ray photoelectron spectroscopy with synchrotron radiation is used to study the interfaces of SiO_2/Si(111), SiO_2/Si(100), Si(111)/Si_3N_4, and SiO_2/Si_3N_4 for device-quality ultrathin gate oxides and nitrides. The thin oxides and nitrides were grown by remote plasma deposition at a temperature of 300 °C. Aftergrowth samples were further processed by rapid thermal annealing for 30 s at various temperatures from 700 to 950 °C. The Si(111)/Si_3N_4 samples were air exposed and formed a thin ~6 Å SiO_2 layer with a Si($2p$) core-level shift of 3.9 eV, thus allowing us to study both the Si(111)/Si_3N_4 and SiO_2/Si_3N_4 interfaces with a single type of sample. We obtain band offsets of 4.54±0.06 eV for SiO_2/Si(111) and 4.35±0.06 eV for SiO_2/Si(100) with film thicknesses in the range 8–12 Å. The Si(111)/Si_3N_4 nitrides show 1.78±0.09 eV valence-band offset for 15–21 Å films. This value agrees using the additivity relationship with our independent photoemission measurements of the nitride–oxide valence-band offset of 2.66±0.14 eV. However, we measure a substantially larger SiO_2/Si_3N_4 ΔE_V value of 3.05 eV for thicker (~60 Å) films, and this indicates substantial differences in core-hole screening for films of different thickness due to additional silicon substrate screening in the thinner (15–21 Å) films. © *1999 American Vacuum Society.* [S0734-211X(99)08904-0]

I. INTRODUCTION

Interfaces of SiO_2/Si(111) and SiO_2/Si(100) have been extremely well studied by photoemission spectroscopy[1–5] but little attention has been given to measurements of the valence-band offsets for ultrathin oxide systems. A crucial issue that continues to inhibit understanding of spectroscopic measurements is sample preparation at the device-grade level of processing such that interface details can be usefully compared to other measurements. In the present study we use ultrathin oxides and nitrides grown on Si(111) and on Si(100) that achieve these interface conditions. Since gate oxide thickness used in current devices has continued to decrease in thickness with corresponding improvements in oxide growth, postgrowth processing and device properties, we decided to reinvestigate the issue of the band offsets for interfaces of SiO_2/Si(111) and SiO_2/Si(100) using current state-of-the-art methods of gate oxide growth. Standard interface capacitance and other electrical measurements done on the same wafer as the electron spectroscopic experiments independently characterized our device-grade samples.[6–8]

II. EXPERIMENTAL DETAILS

A. Film preparation methods

Native oxide layers on Si(111) substrates were removed by etching in 40 wt % NH_4F for 4 min and then rinsing for 20 s with deionized water. The Si(100) wafers were treated with 1 wt % HF and also rinsed in de-ionized water for 20 s. These steps produced H-terminated Si surfaces. After this

a)Electronic mail: jkeister@unity.nesu.edu

step, the wafers were loaded into the vacuum chamber. The films were then grown by one of three methods.

1. Method 1

Ultrathin SiO_2 samples were made using remote plasma-enhanced (RPE) oxidation. Wafers of Si(111) or Si(100) were heated to 300 °C and exposed to a flow of excited oxygen formed in a remote He/O_2 rf plasma. The He and O_2 were flowed at 200 and 20 sccm ($cm^3\,min^{-1}$), respectively, at a total chamber pressure of 0.3 Torr, with the 13.56 MHz rf plasma power fixed at 30 W. On-line (i.e., *in situ*) Auger electron spectroscopy (AES) measurements characterized the growth rate as following a power law SiO_2 film thickness dependence on time: $t_{ox} \approx 7t^{0.28}$ (where t_{ox} is the SiO_2 thickness in Å and t is plasma exposure time in minutes).[9] The SiO_2 films reported in this study [measured by soft x-ray photoelectron spectroscopy (SXPS) to be in the range 9–22 Å] were made using exposure times of approximately 5 s to nearly 10 min.

2. Method 2

Remote plasma-enhanced chemical vapor deposition (RPECVD) of SiO_2 to produce thicker (~80 Å) films. These were produced by flowing dilute silane downstream from the oxygen plasma. After passing the plasma excitation, excited O_2 flowed through a rf ring of 2% SiH_4 in helium. The wafers were found to grow at ~34–40 Å per minute at a wafer temperature of 300 °C. The chamber pressure was maintained at 0.3 Torr during growth. Flow rates were: 200 sccm He, 20 sccm O_2, and 10 sccm of the 2% SiH_4 mixture.

3. Method 3

RPECVD was also used to produce (hydrogen-rich) Si_3N_4 films ranging in thickness from 10 to 80 Å. Excited N_2 from the He plasma was flowed through a ring of SiH_4. The wafers were observed to grow at a rate of ~6–8 Å/min at a wafer temperature of 300 °C. The chamber pressure was maintained at 0.2 Torr during growth. Flow rates were: 200 sccm He, 60 sccm N_2, 10 sccm of the 2% SiH_4 mixture. When these samples were exposed to air, reaction with atmospheric water produced a native silicon oxide overlayer (~5–10 Å thickness), presumably by the substitution reaction:

$$-NH-+H_2O \rightarrow -O-+NH_3. \quad (1)$$

After growth, some of the samples were subjected to *ex situ* rapid thermal annealing (RTA) using optical heating in an Ar atmosphere. In many cases, a single oxidized wafer was broken *ex situ* and fragments were annealed at various temperatures in the range 600–950 °C by RTA (for 30 s) in Ar, providing a means of comparing "as grown" and annealed samples under the same oxidation conditions.

The films were transferred under air to the ultrahigh vacuum XPS chamber of NSLS-U4A. Once in vacuum, the samples were annealed at ~500 °C by electron-beam heating of the metal sample holder. This removes contamination due to weakly bonded adsorbates picked up in air. The thick nitride films were further treated with neon ion etching (5 min at 500 eV beam energy, 3×10^{-5} Torr chamber pressure) to remove some of the SiO_2 overlayer. Then, a second ~600 °C anneal was performed after the etching in order to reequilibrate the film somewhat.

B. Soft x-ray photoemission spectroscopy (SXPS) measurements

The SXPS configuration at the U4A beamline of the National Synchrotron Light Source (NSLS) includes a 6 m toroidal grating monochromator which produces a photon beam with ≤0.2 eV resolution at photon energies ($h\nu$) of 10–200 eV.[9,10] At 130 photon energy this system has ~0.15 eV total resolution, photons, and electrons. The photoelectron kinetic energy (KE_e) was measured with a 100 mm hemispherical analyzer fixed at 45° to the photon beam axis. All the spectra presented here were obtained with the sample surface facing the analyzer at the normal emission geometry (α=90° take-off angle). The room temperature SXPS spectra were collected with the sample holder grounded, and the electron analyzer was used in fixed pass energy mode with a resolution of ~0.1 eV.

The Fermi energy E_F was used as the reference energy and was measured using a metal sample attached to the same sample holder. The E_F threshold appeared at a kinetic energy of 4.6 eV less than the photon energy. Valence-band offsets were measured within each spectrum individually and were not affected by any small offset bias applied to the sample. The sample SiO_2 film thickness was estimated from the Si($2p$) SXPS SiO_2 and substrate peak intensity ratio, as described elsewhere,[11] and were consistent with independent *in situ* (on-line) AES and ellipsometric measurements within experimental uncertainties.

III. RESULTS

A. Valence-band offsets for thin SiO_2 films on Si(111) and Si(100)

Because of the surface sensitivity of SXPS, the Si substrate signal can be seen only for thin films. Thus, the Si–SiO_2 valence-band offset ΔE_V was measured using thin RPE oxidation SiO_2 films of 10±2 Å thickness. This film thickness was measured from the core-level peak intensity ratio between Si and SiO_2 Si($2p$) peaks [binding energy (BE, (Si) ~99.3 eV)] which are distinct due to the ~4 eV chemical shift difference in BE (SiO_2) ~104 eV. As shown in Fig. 1, the valence band spectra for such films show the same features despite being obtained using different photon energies. The differences can be explained as: (i) Auger transitions which have fixed electron energies, or (ii) intensity changes due to energy-dependent electron escape depths. These spectra are dominated by a signal attributable to oxygen atoms in the SiO_2 film. The O($2s$) peak at binding energy ($h\nu$−KE)~26 eV can clearly be distinguished from the O($2p$) peak at 7 eV (with additional components at ~11 and 14 eV). The onset of the O($2p$) signal at BE ~4 eV corresponds to the valence band maximum (E_V) of the SiO_2 film.

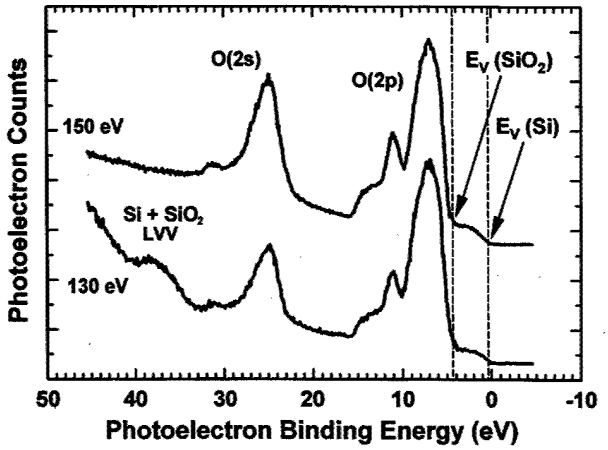

FIG. 1. Typical valence band scans for a thin (~15 Å) SiO_2 film grown on Si(111) substrate. Shown are spectra acquired at 130 and 150 eV photon energy. The higher energy shows more substrate signal (BE <4 eV) due to increased electron escape depth. The lower energy scan shows greater scattered electron background as well as silicon Auger signal near 90 eV electron kinetic energy. The small peak near 31 eV binding energy is Ta($4f$) XPS signal from the tantalum wire which was used to hold the silicon wafer fragment to the sample holder.

The signal at lower binding energy results from the Si substrate, which has an onset BE of nearly zero as shown in Fig. 1.

The difference between these two onsets corresponds directly to the valence-band offset of the interface. That is, $\Delta E_V = E_V(\mathrm{Si}) - E_V(\mathrm{SiO_2})$. Thus, we have measured ΔE_V by fitting the low-binding-energy part of the spectrum with two broadened step functions. In Fig. 2 is shown the edge region of an SXPS spectra obtained at 130 eV photon energy for a SiO_2 film of 10 Å thickness grown on Si(111). We have found that the spectrum in this region is well modeled by a pair of Gaussian-broadened Fermi functions (the Fermi width is virtually negligible in this case compared with the Gaussian component), with a parabolic peak added to match the signal found experimentally just below the Si band edge.

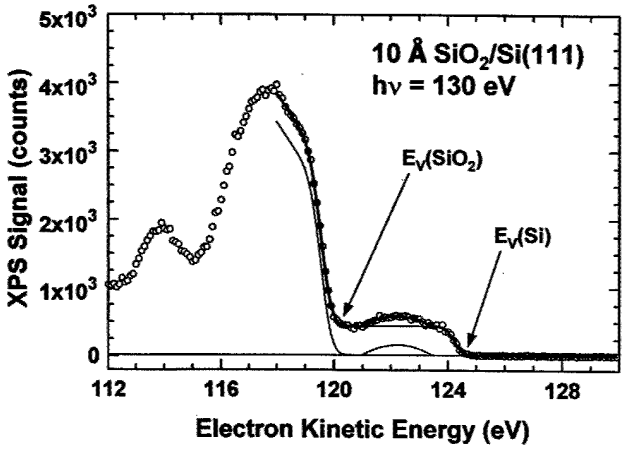

FIG. 2. Closeup view of the silicon and silicon dioxide valence-band edges measured for a 10 Å SiO_2 film grown on Si(111) substrate using a photon energy of 130 eV. The fitting functions are described in the text.

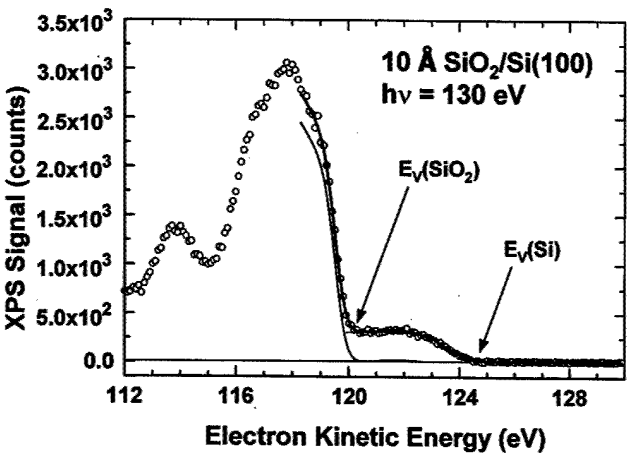

FIG. 3. Closeup view of the silicon and silicon dioxide valence-band edges measured for a 10 Å SiO_2 film grown on Si(100) substrate using a photon energy of 130 eV. The fitting functions are described in the text.

Fits such as these, made using samples of similar thickness and various postoxidation anneal temperatures, were used to derive an average value for ΔE_V of the thin SiO_2/Si(111) interface of 4.54±0.06 eV. ΔE_V was found to be quite constant independent of annealing. Similarly, we have fit the valence-band edge spectra for thin SiO_2 films on the Si(100) substrate. These spectra are similar (see Fig. 3), but with two distinct differences (i) the parabolic peak is much less for the Si substrate, and (ii) onset for Si bulk is much broader, at nearly twice the width of the peaks encountered so far (~1.5 eV compared to 0.7 eV). Again, the ΔE_V values obtained appear independent of annealing treatment, but show a distinct substrate-orientation dependence as pointed out by Alay and co-workers.[12] For ~10 Å SiO_2/Si(100) we find $\Delta E_V = 4.35 \pm 0.06$ eV, which is 0.19±0.08 eV lower than for Si(111). Quantitatively these results compare favorably with previous work (see Table I). However, the present work is done with better resolution and device-proven processes, so we believe our work to be superior.

This direct measure of the valence-band offset can be compared with an indirect approach as well.[13] In particular, this ΔE_V value can be used in conjunction with $(E_V - E_{CL})$ values (the electron energy difference between Si($2p$) core level peak and valence band edge) measured for thin and thick SiO_2 films, in order to derive a Si–SiO_2 core level shift comparable to known values.[1,2,11] The estimated ΔE_{CL} value is given by:

TABLE I. Compared band offset measurements (values are given in eV).

Value	Si(100)	Si(111)	ΔSi(100)–Si(111)
ΔE_V	4.3[a]	4.5[b]	
(eV)	4.43 wet[c]	4.36 (dry)[c]	0.13[c]
	4.49 dry[c]		
	4.54±0.06 eV[d]	4.35±0.06[d]	0.19±0.08[d]

[a]Reference 2.
[b]Reference 1.
[c]Reference 12.
[d]Present work.

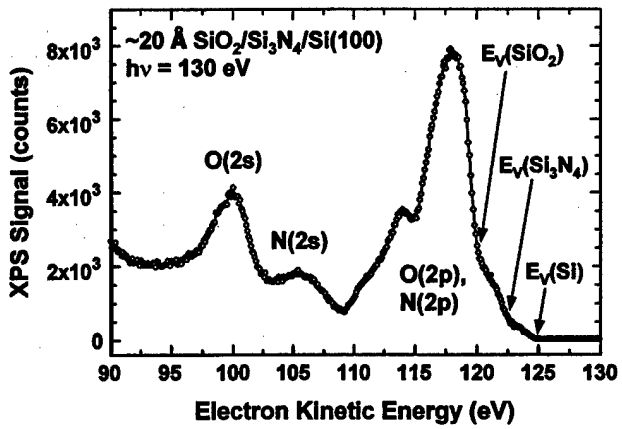

FIG. 4. Valence-band scan measured at 130 eV photon energy for a ~20 Å Si_3N_4 film deposited on Si(100) using the RPECVD method. A silicon dioxide overlayer resulting from atmospheric exposure is the dominant feature. In addition, the Si_3N_4 valence-band edge appears between those of silicon substrate and SiO_2. The N(2*s*) peak at ~106 eV kinetic energy is evident, and resembles the O(2*s*) peak at ~100 eV.

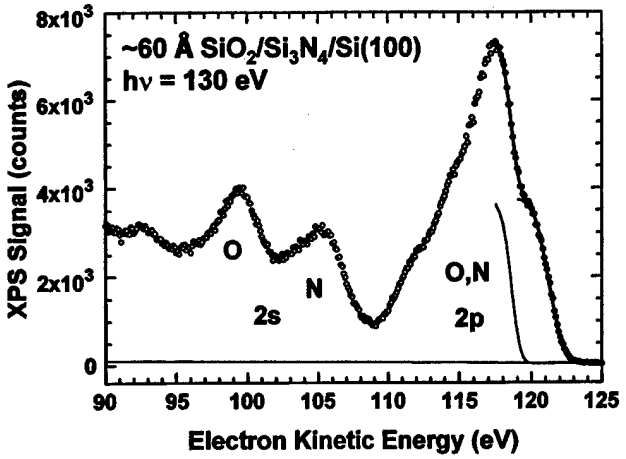

FIG. 5. Valence-band scan measured at 130 eV photon energy for a ~60 Å Si_3N_4 film deposited on Si(100) using the RPECVD method. This film is quite thick compared to the electron escape depth (~5–10 Å) so that no substrate signal is seen. The large valence-band offset for SiO_2/Si_3N_4 measured from this spectrum differs from that measured for thinner films, in part due to photoelectron hole screening by silicon substrate.

$$\Delta E_{CL}=\Delta E_V(\mathrm{Si/SiO_2})+(E_V-E_{CL})(\mathrm{SiO_2})-(E_V-E_{CL})(\mathrm{Si}). \quad (2)$$

We can average the Si(111) and Si(100) results for ΔE_V to give 4.44 eV, and obtain an average value of (E_V-E_{CL})(Si) of 98.52 eV by using data for the same thin (~10 Å) SiO_2 film samples. For the $(E_V-E_{CL})(SiO_2)$ value we turn to a thick film of SiO_2 (~80 Å) which yields 98.45 eV. The derived ΔE_{CL} value of 4.37 eV compares very well with a ΔE_{CL} value of 4.36 eV estimated for a 80 Å film using the core-hole screening approach.[11]

B. Valence-band offsets for thin Si_3N_4 films

We have also measured valence-band offsets for silicon nitride films deposited on Si(111) and Si(100) substrates. An example of such valence-band data for <20 Å Si_3N_4 films on Si(100) is shown in Fig. 4. The hydrogen-rich silicon nitride (made by RPECVD, using N_2^* and SiH_4) is known to react readily with atmospheric water to produce a surface layer of silicon (di) oxide. Thus, the spectra show three distinct offsets: (i) Si substrate, (ii) Si_3N_4, and (iii) SiO_2. We have used these data to measure ΔE_V for the Si_3N_4/Si interface. Unfortunately, the overlapping spectra in this case makes the Si_3N_4/Si offset ΔE_V less clear. In addition, the Si_3N_4 onset was not sharp enough to measure for many films thinner than ~16 Å. From the best of such data, we arrive at an average value for ΔE_V (Si_3N_4/Si) of 1.78±0.09 eV for an average total film thickness (oxide and nitride) of 18±3 Å. We could not find any statistically significant differences between samples of difference substrate orientation or annealing treatment.

We can estimate the Si_3N_4/SiO_2 valence-band offset from these data as well. Again, using a pair of broadened step functions, we have fit the nitride and oxide onsets from the spectra and found an average Si_3N_4/SiO_2 valence-band offset of 2.66±0.14 eV. It is comforting to find that the ΔE_V values measured independently for Si–SiO_2, Si–Si_3N_4, and SiO_2–Si_3N_4 follow a simple additivity rule: i.e., $\Delta E_V(\mathrm{Si–SiO_2})=\Delta E_V(\mathrm{Si–Si_3N_4})+\Delta E_V(\mathrm{Si_3N_4–SiO_2})$. In this case, adding the two nitride-relative offsets 2.66 and 1.78 eV yields 4.44 eV which is precisely the average of the ΔE_V values for the SiO_2 films on the two crystal faces (4.45 ±0.09 eV). However, when we measure the SiO_2–Si_3N_4 ΔE_V value from spectra of thicker films (~60 Å), we find it much higher (see Fig. 5). The ΔE_V value of 3.06 eV measured from the spectra in this figure may be higher due to the screening effect difference for different oxide overlayer thickness, as discussed below.

IV. DISCUSSION AND CONCLUSIONS

The valence-band offsets for silicon/silicon oxide and silicon/silicon nitride have been measured with good accuracy using soft x-ray photoemission. These values are critical in the design of oxide-semiconductor devices. In agreement with previous workers, we have found a difference in valence-band offset between the Si(100) and Si(111) crystal interfaces with silicon dioxide. This can be correlated with the number and type of other species at the interface, such as dangling bond defects or hydrogen.[14] This interpretation would suggest that the Si(111) interfaces have less interface H, assuming no dangling bonds. A second explanation for the ΔE_V difference is the orientation of the interface bond dipoles relative to the surface normal. The interface bond dipole is more aligned with the surface normal for the (111) orientation and less aligned (more glancing) for the (100) orientation. If the contribution of the interface bond dipole to the valence-band offset (total interface dipole) follows a cosine rule, this would also explain the lower ΔE_V for Si(100)/SiO_2 relative to Si(111)/SiO_2.

The silicon nitride valence-band edge has also been measured relative to those of Si bulk and SiO_2. These values appear to be less sensitive to the underlying Si crystal orien-

tation. The Si_3N_4–SiO_2 ΔE_V has been found to be somewhat film thickness dependent, increasing by ~0.4 eV between 18 and 60 Å film thicknesses. This can be explained as a result of core-hole screening by image charge in the higher k silicon substrate. In other words, the high dielectric constant ϵ_{opt} mismatch ($\Delta\epsilon_{opt}=12-2=10$) between silicon and the SiO_2 substrate is likely to be responsible for this shift. The mismatch is about half as great in the case of screening by the Si substrate of silicon nitride ($\Delta\epsilon_{opt}=12-7=5$). This screening effect causes lower binding energies for thin films and higher binding energies in thicker films.

The results presented here can be used to derive values for the conduction-band offsets as well, using the known E_g values. For example, the known SiO_2 gap energy of 8.95 eV[15] implies a Si–SiO_2 ΔE_C of 3.38 eV (using the average ΔE_V of 4.44 eV and Si bandgap of 1.1 eV).

ACKNOWLEDGMENTS

This work was supported, in part, by DOE-Office of Basic Energy Sciences, by NSF, by NRC, by the Office of Naval Research, and the Army Research Office.

[1]F. J. Grunthaner and P. J. Grunthaner, Mater. Sci. Rep. **1**, 65 (1986).
[2]F. J. Himpsel, F. R. McFeely, A. Taleb-Ibrahimi, J. A. Yarmoff, and G. Hollinger, Phys. Rev. B **38**, 6084 (1988).
[3]M. M. Banaszak-Holl, S. Lee, and F. R. McFeely, Appl. Phys. Lett. **65**, 1097 (1994).
[4]K. Z. Zhang, M. M. Banaszak-Holl, J. E. Bender, S. Lee, and F. R. McFeely, Phys. Rev. B **54**, 7686 (1996).
[5]F. R. McFeely, K. Z. Zhang, M. M. Banaszak-Holl, S. Lee, and J. E. Bender, J. Vac. Sci. Technol. B **14**, 2824 (1996).
[6]H. Niimi and G. Lucovsky, Surf. Coat. Technol. **98**, 1529 (1998).
[7]H. Niimi, K. Koh, and G. Lucovsky, Proc. Electrochem. Soc. **12**, 623 (1996).
[8]G. Lucovsky, H. Niimi, Y. Wu, C. R. Parker, and J. R. Hauser, J. Vac. Sci. Technol. A **16**, 1721 (1998).
[9]P. Thiry, P. A. Bennett, S. D. Kevan, W. A. Royer, E. E. Chaban, J E. Rowe, and N. V. Smith, Nucl. Instrum. Method Phys. Res. **222**, 85 (1984).
[10]G. K. Wertheim, J. E. Rowe, D. M. Riffe, and N. V. Smith, AIP Conf. Proc. **215**, 259 (1990).
[11]J. W. Keister, J. E. Rowe J. J. Kolodziej, H. Niimi, H.-S. Tao, T. E. Madey, and G. Lucovsky J. Vac. Sci. Technol. A (submitted).
[12]J. L. Alay and M. Hirose, J. Appl. Phys. **81**, 1606 (1997).
[13]E. T. Yu, M. C. Phillips, J. O. McCaldin, and T. C. McGill, J. Vac. Sci. Technol. B **9**, 2233 (1991).
[14]P. Perfetti, C. Quaresima, C. Coluzza, C. Fortunato, and G. Margaritondo, Phys. Rev. Lett. **57**, 2065 (1986).
[15]S. Miyazaki, H. Nishimura, M. Fukuda, L. Ley, and J. Ristein, Appl. Surf. Sci. **113/114**, 585 (1997).

Photoelectron spectroscopy studies of growth, thermal stability, and alloying for transition metal-tungsten (111) bimetallic systems

J. J. Kolodziej* and T. E. Madey†
The Department of Physics and Astronomy and Laboratory for Surface Modification, Rutgers, The State University of New Jersey, Piscataway, New Jersey 08854-8019

J. W. Keister and J. E. Rowe
Physics Department, North Carolina State University, Raleigh, North Carolina 27695
(Received 22 February 2001; published 28 January 2002)

High-resolution soft-x-ray photoelectron spectroscopy using synchrotron radiation is used to study late-transition-metal films (Pt, Pd, Ir, Rh) on W(111). It is found that the films grow in a layer mode at 300 K. A single physical monolayer (ML) of each of these metals "floats" on the tungsten substrate and, upon annealing to $T>700$ K, the metal film-coated W(111) becomes faceted, i.e., covered with three-sided pyramids exposing {211} planes. During growth of Pt, Ir, and Rh films, at 300 K, for coverages exceeding 1 ML, atomic mixing at the interface is observed, driven by energy released in the adsorption process. Multilayer films of these metals on W(111), upon annealing, undergo complex transformations which include alloying, segregation, cluster formation, and faceting of the surface between clusters. It is demonstrated that despite the unusual complexity of the problem, soft-x-ray photoelectron spectroscopy allows for successful investigation of these transformations.

DOI: 10.1103/PhysRevB.65.075413 PACS number(s): 68.55.−a, 68.60.Dv, 64.75.+g, 81.05.Bx

I. INTRODUCTION

High-resolution core-level photoemission spectroscopy is extremely useful in studies of complex bimetallic systems for which, during formation, many concurrent phenomena such as alloying, surface segregation, cluster formation, or surface reconstruction may occur. Despite many challenges with data interpretation, high-resolution soft-x-ray photoelectron spectroscopy (SXPS) is a very useful technique for studies of bimetallic interfaces since it provides identification of the surroundings of various atoms via measurements of core-level shifts.

Transition metals, their alloys, and thin films have attracted much attention recently, both because they have interesting physical properties, and because of the variety of their technological applications as catalysts, shape memory alloys, and in new magnetic materials. As shown recently, the atomically rough tungsten (111) surface covered with films of certain metals (Pt, Pd, Rh, Ir, Au) and annealed to temperatures 700–800 K undergoes massive reconstruction to form three-sided pyramids of nanometer scale dimensions with {211} planes as facet sides.[1,2] This evidence for instability of surface morphology in a bimetallic system has important implications: effective control over growth and morphology of nanostructure features on surfaces is essential for the design and operation of future generations of devices.

In previous studies we have reported on growth and alloying of late-transition-metal films on the tungsten (211) surface.[3,4] In the present work we focus on the growth and thermally activated restructuring (faceting) induced by late-transition-metal films on atomically rough tungsten (111). It is demonstrated that the extremely complex structures present on these bimetallic surfaces may be successfully resolved and investigated with the SXPS technique.

Specifically, in the present study, we report high-resolution $4f_{7/2}$ photoemission spectra from $5d$- and $4d$-late-transition-metal (Pt, Pd, Ir, Rh) covered tungsten surfaces as a function of coverage and annealing temperature. Where possible (Pt and Ir on W), admetal $4f$ core-level spectra have been measured and correlated with the substrate spectra.

There are several interesting findings in these studies of metals on W(111). First, we report evidence for segregation of single monolayers of Pt, Pd, Ir, and Rh on the atomically rough W(111) surface upon annealing [in contrast to reports of surface alloys on planar W(100) under certain conditions; cf. Refs. 5 and 6]. Second, we find strong evidence for intermixing at the interface for multilayer deposition of several metals (Pt, Rh, Ir) on W(111) at room temperature. This is unexpected for the thin-film community; it has been generally believed that thin films of high-melting-T metals form abrupt interfaces.

The present results have implications beyond the specific systems studied. Rapidly developing highly accurate first-principles theoretical methods for solid-state energetics allow now for precise description of bulk and surface properties of materials (cf. Refs. 7–10). For example, a comprehensive table of segregation energies for transition-metal impurity monolayers on close-packed surfaces of transition metals has been published recently.[11] We believe the time is ripe for careful examination of phenomena occurring at interfaces and surfaces of bimetallic systems with highly surface-sensitive techniques, in order to test and to stimulate further theoretical work.

This paper is organized as follows. After the description of experimental procedures we present results and data analysis for four different metallic overlayers (Pt, Pd, Ir, Rh) on W(111); all of these metals are known to induce faceting of W(111) to {211}. The Pt/W(111) data are described in greatest detail to illustrate the analysis and curve-fitting pro-

cedures. The essential features of the remaining three overlayers are presented more briefly. Finally all of the data are discussed to analyze the film growth, thermal stability, segregation, and alloy formation. The findings for W(111)-based bimetallic systems (similarities as well as strong differences) are compared with the earlier study of W(211)-based systems.

II. EXPERIMENTAL METHODS

The experiments have been performed in a stainless-steel ultrahigh-vacuum experimental system at the National Synchrotron Light Source of Brookhaven National Laboratory, on beamline U4A. Details of the experimental setup are described elsewhere.[12] The total spectral resolution is ~0.2 eV at 150 eV and below 0.1 eV at 80 eV photon energy. Typically the x-ray beam and the energy spectrometer axis form an angle of 45° and the x-ray beam is incident at 45° onto the sample. The photon flux is monitored and the measured spectra are normalized to account for the slowly changing photon flux. The tungsten (111) substrate is prepared by repetitive heating in oxygen (1×10^{-7} Torr) at 1300 K, followed by an abrupt increase of substrate temperature to 2300 K for a few seconds (flash). The experimental setup contains several metal dosers used for deposition of platinum, palladium, rhodium, iridium, and gold. Special care is taken to outgas the dosers before their use. Dosers are shielded during operation by cooled surfaces and the background pressure during operation does not exceed 2×10^{-10} Torr. Details of the coverage calibration have been described in Refs. 3 and 4. Sample temperature is measured by a W5%Re–W26%Re thermocouple spot-welded to the side of the W crystal.

In order to investigate thermally activated processes occurring on overlayer films and at the interface, stepwise annealing to increasingly higher temperatures is used: after metal deposition the sample is annealed in a sequence of increasing temperatures ranging from 400 to 2300 K. After each step the sample is cooled, and SXPS data are recorded.

III. RESULTS AND DATA ANALYSIS

A. Platinum

1. Film growth

In Fig. 1, a sequence of SXPS spectra associated with the growth of a Pt film on the W(111) surface is shown. The Pt $4f_{7/2}$ peak shape is distinctly different for coverages of 1/3, 2/3, and 1 ML [where one physical monolayer (ML) is defined as the coverage needed to shadow all substrate atoms: $\sim1.7\times10^{15}/\text{cm}^2$]. This is a simple consequence of the structure of a single pseudomorphic monolayer on bcc (111) and a layer-by-layer film growth. The pseudomorphic layer on a bcc (111) crystal surface contains three geometrical "layers" containing atoms in different chemical configurations.[13] A complete adlayer (1 ML) contains equal numbers of atoms of all three types. We have performed a decomposition of Pt peaks using as model functions Doniach-Sunjic (DS) line shapes. The $4f_{7/2}$ feature, as demonstrated in Fig. 2, is single-component at 1/3 ML, double-component at 2/3 ML,

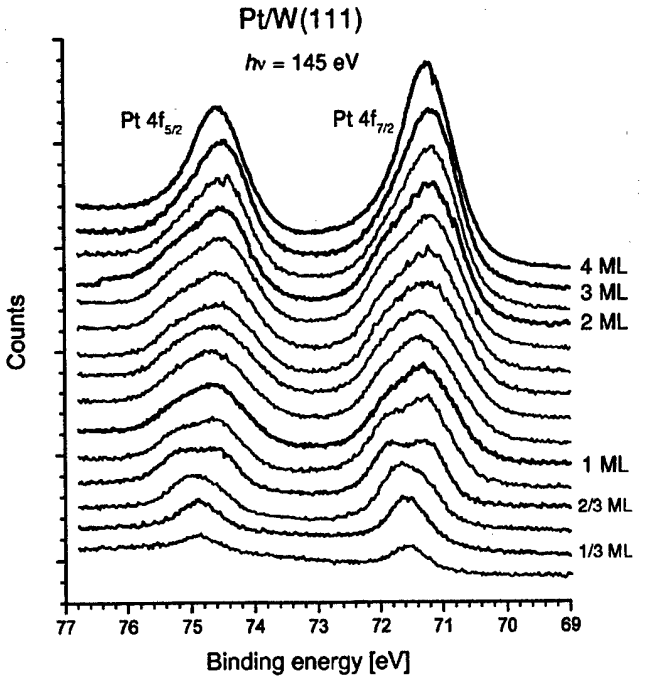

FIG. 1. The Pt $4f$ spectral region recorded during growth of Pt films on W(111) at 300 K.

and triple-component at 1 ML. All components have comparable intensity. Such an evolution of the Pt SXPS peak evidences a layer-by-layer character of growth (in the sense of geometrical "layers"). For higher (multilayer) coverages the Pt $4f_{7/2}$ feature is smooth and shapeless. This is very different from the case of a pseudomorphic film on W(211) (Ref. 4) where the single DS lines could be associated with physical layers at the interface and at the surface. In contrast, for a Pt film on W(111), there are differences in positions of SXPS lines associated with different geometrical layers within the same physical layer at the interface and at the surface. Thus the $4f_{7/2}$ SXPS feature for a Pt pseudomorphic film on W(111) is composed of slightly shifted multiple components and unique decomposition of the $4f$ feature is not possible. This is illustrated in Fig. 2(d) where a very accurate Doniach-Sunjic lines fit produces an unphysical surface-to-bulk components ratio (approximately 1:1 is expected based on photoelectron attenuation length). As illustrated in the inset in Fig. 3, the dependence of the substrate W $4f$ peak intensity on the film thickness is exponential. Since one dose corresponds to approximately 1-ML coverage it is difficult to judge whether the growth is a true layer-by-layer or random ("sticks-where-it-hits") growth mode. On the other hand the low-energy electron-diffraction (LEED) image remains 1 $\times$1 during growth but spot sharpness deteriorates with increasing coverage. These observations indicate that the Pt deposit uniformly covers the W substrate, however, the surface of the film is not atomically flat. [In order to illustrate the difference in attenuation of substrate signal for the flat and the 3d growth mode we included an attenuation curve for Fe on W(111) growth, see the inset in Fig. 3. The Fe on W attenuation is characteristic of $3d$ growth above 2-ML (two doses) coverage. The Pt on W attenuation is characteristic of flat growth.]

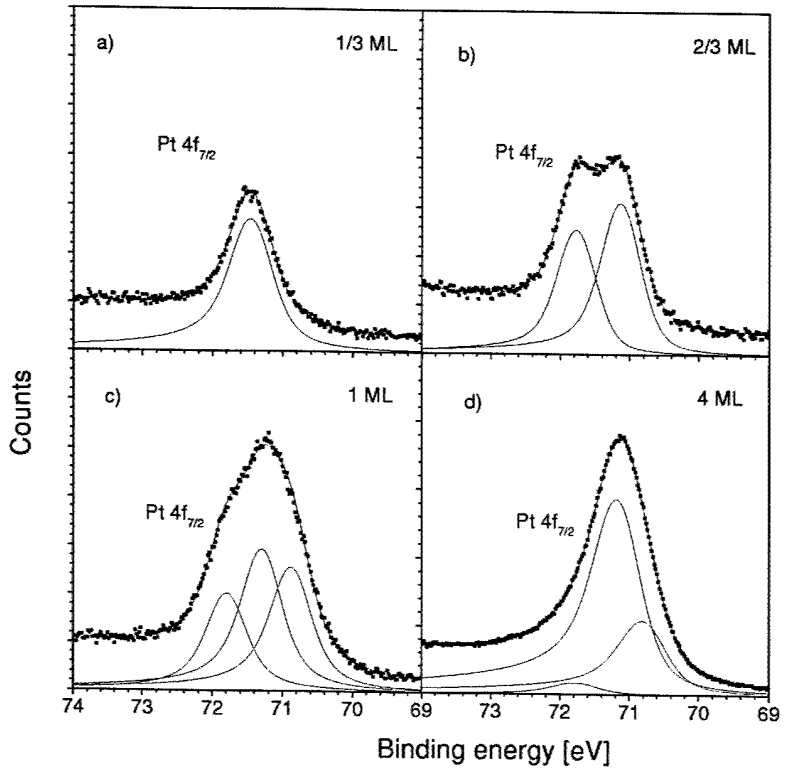

FIG. 2. Doniach-Sunjic (DS) Pt $4f_{7/2}$ lineshape fits for a few different thicknesses of a Pt film on W(111): (a) for 1/3-ML, (b) for 2/3-ML, (c) for 1-ML, and (d) for 4-ML coverage.

A very interesting property of the Pt/W(111) system observed during growth of a Pt film at room temperature is that satellite peaks appear in the W $4f$ region after single-monolayer coverage is exceeded. These peaks are shifted by ~ 1 eV to higher binding energy, relative to W $4f$ bulk peaks (see Fig. 3). These peaks have been previously assigned to a tungsten impurity in the Pt host (or a dilute W alloy)[4] and their presence during adsorption of Pt on W(111) provides evidence that mixing at the Pt/W interface occurs as a result of the adsorption process. It can be seen that for lower coverages (2–3 ML) the satellite W $4f_{7/2}$ peak is slightly shifted relative to the dilute W in the Pt $4f_{7/2}$ peak (the Pt film is too thin and the strict "dilute" situation is not possible). Above 3-ML coverage the additional peak appears at the exact position of the "dilute alloy" peak which is shifted by 0.95 eV with reference to the bulk W position (Ref. 4). The intensity of the dilute alloy peak relative to the intensity of the substrate peak increases until a coverage of 6 ML is reached. This indicates that the mixing at the interface continues up to 6-ML coverage.

2. *Annealing of Pt films*

The thermal evolution of the W(111) surface covered with 1 ML of Pt has been monitored by LEED and SXPS (see Fig. 4). Each SXPS spectrum shown in Fig. 4 is labeled with the corresponding type of surface reconstruction as determined by LEED. As-dosed Pt $4f$ peaks display shoulders on the high binding-energy side, resulting from their multicomponent character as discussed above. Below 500 K the film maintains 1×1 structure. Above 500 K the Pt SXPS peaks lose their distinct shoulders and LEED indicates a $(2\sqrt{3}\times2\sqrt{3})R30°$ reconstructed surface. This configuration is

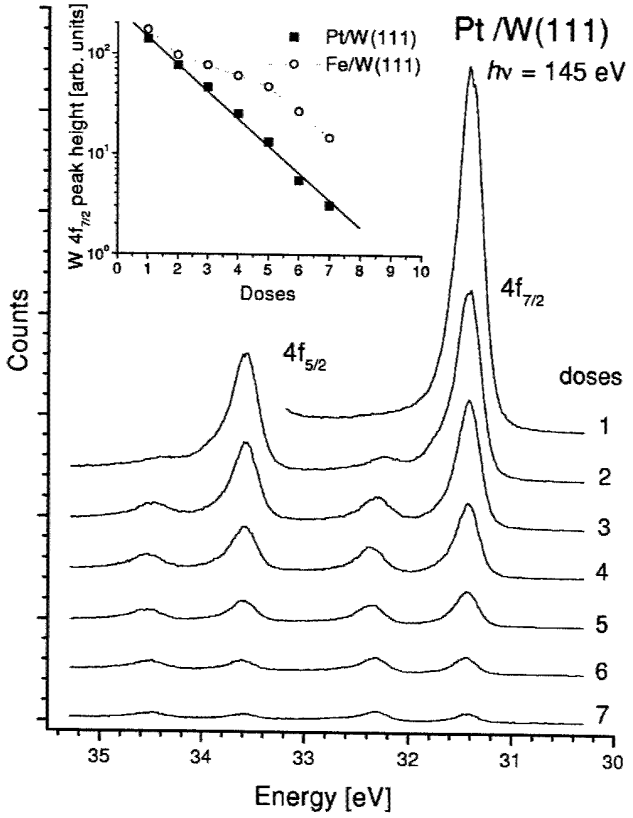

FIG. 3. W $4f$ spectra associated with growth of a multilayer Pt film on W(111) at room temperature. The inset shows the height of the W $4f_{7/2}$ peak as a function of coverage. One dose corresponds to ~ 1 ML (solid line, square points). For comparison we show the attenuation curve for a case when the flat growth mode breaks down at ~ 2-ML coverage [case of Fe/W(211): dotted line, circle points].

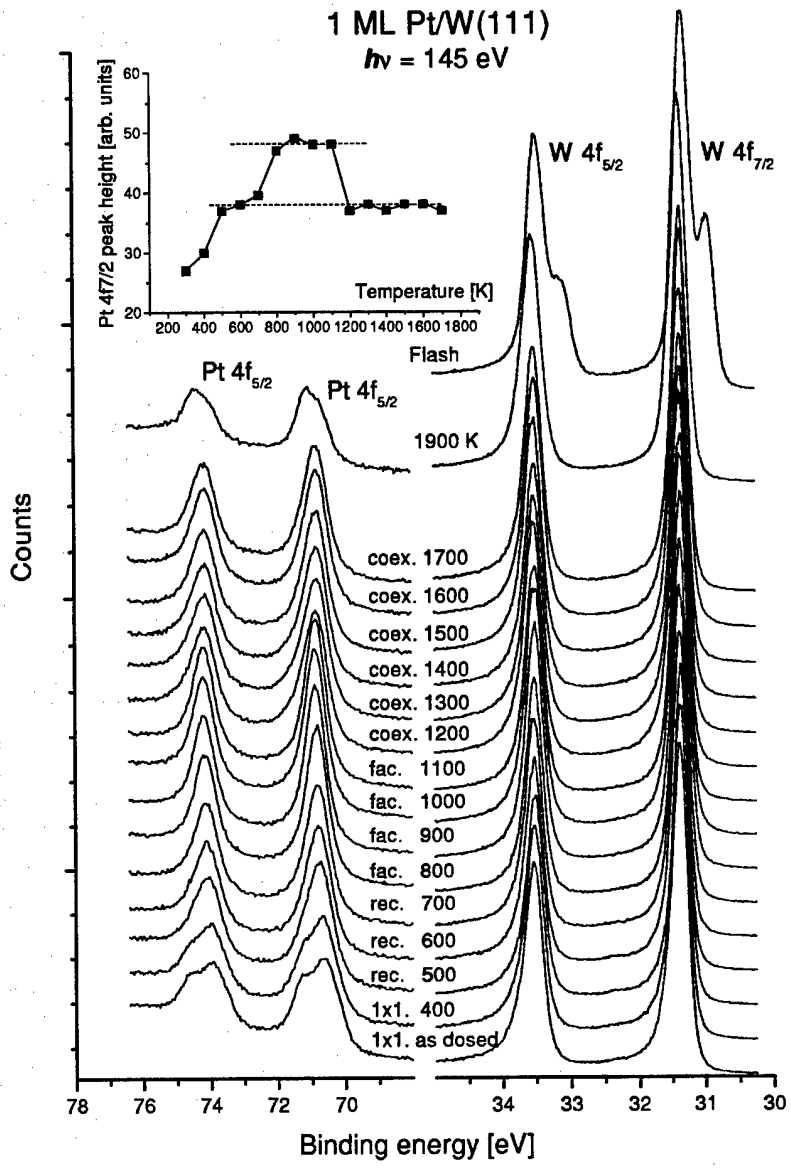

FIG. 4. Annealing sequence for a 1-ML Pt film on W(111). The Pt 4*f* and W 4*f* spectral regions are shown following annealing to the indicated temperature for 1 min. The meanings of reconstruction labels are the following: "rec.," $(2\sqrt{3}\times 2\sqrt{3})R30°$, "fac.," faceted, and "coex," coexistence of faceted and "rec." The inset shows a Pt $4f_{7/2}$ peak height as a function of annealing temperature.

stable up to a temperature of ~700 K where the faceting surface phase transition occurs. The faceting transition can be identified both by a change in the LEED pattern (see Refs. 14 and 15 for a description of the "faceted" LEED pattern) and by narrowing of the Pt 4*f* feature, which is an effect of a change in the Pt peak characteristic of a planar Pt adlayer on W(111) (multicomponent) to that characteristic of a Pt adlayer on W(211) (single component). (Facets are 10–100 nm in size and their edges make little contribution to the SXPS peak intensity.) This is visualized in Fig. 4 (inset) which shows the height of the Pt $4f_{7/2}$ peak as a function of annealing temperature. The narrowing of the Pt feature results in increased height of the feature. The plateau between 700 and 1100 K is correlated with the faceted LEED pattern. Above 1100 K the Pt $4f_{7/2}$ peak height decreases and the LEED pattern becomes mixed [faceted and $(2\sqrt{3}\times 2\sqrt{3})R30°$] suggesting the coexistence of faceted and planar regions on the surface. In the W $4f_{7/2}$ region no changes in the peak shape and intensity are seen throughout the whole annealing temperature range. Above the thermal-desorption threshold for Pt, W 4*f* features associated with surface tungsten atoms appear (see also Refs. 16 and 17).

In Fig. 5, Pt 4*f* and W 4*f* spectra associated with annealing of a 5-ML thick Pt film on W(111) are shown. For temperatures below 1000 K the observed peak changes resemble those observed during annealing of the Pt/W(211) system.[4] Peaks in the W 4*f* region do not change [see the W $4f_{7/2}$ dilute alloy peak formed upon Pt adsorption at the 32.35-eV binding energy (BE) and the substrate peak at 31.4 eV] up to an annealing temperature of 600 K. Above this temperature the dilute alloy peak increases in intensity and above 800 K it shifts towards the substrate peak, evidencing formation of a saturated alloy. In the dilute alloy phase Pt 4*f* peaks appear unchanging (since the number of Pt atoms in contact with W atoms is low), but the alloy saturation is accompanied by shifts of Pt features to higher binding energy, and by splitting into two separate components (at ~72.4-eV BE which we attribute to the Pt in the Pt/W alloy and at 71.5-eV BE attributed to the Pt segregated to the alloy surface). Above 1000 K there is a significant increase in the intensity

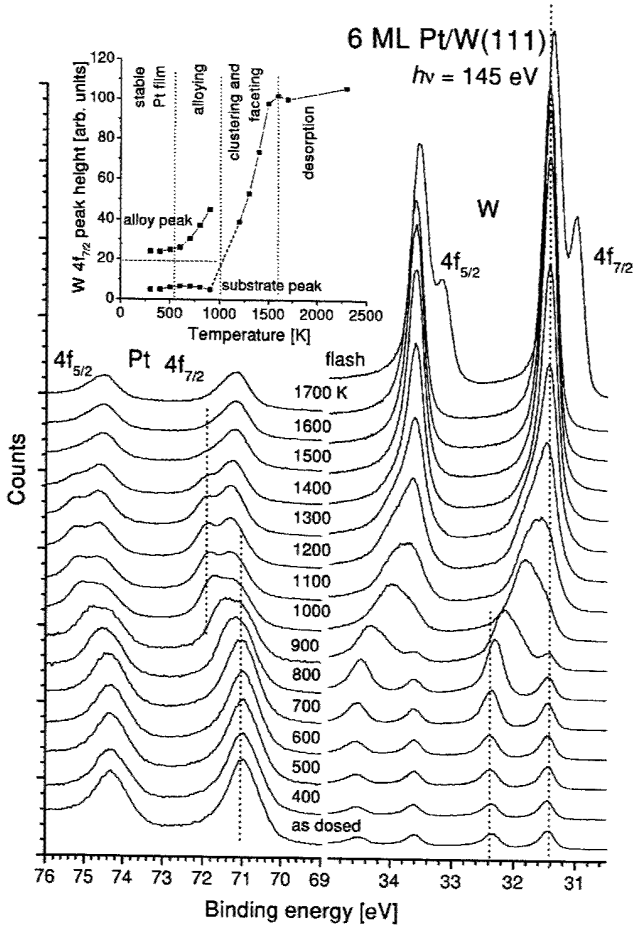

FIG. 5. Pt $4f$ and W $4f$ SXPS spectra associated with the annealing sequence for a 6-ML Pt film on W(111). Annealing time is 1 min. The inset shows the intensity of substrate and dilute alloy W $4f_{7/2}$ peaks as a function of temperature.

of the W $4f_{7/2}$ substrate peak and a decrease in the intensity of the Pt $4f_{7/2}$ alloy peak at 72.4-eV BE. This peak becomes invisible at 1500 K, i.e., ~200 K below the threshold temperature for thermal desorption of Pt from the Pt-W alloy.[18] These observations indicate that upon annealing to $T > 1100$ K the alloy film evolves into three-dimensional clusters whose areas exposed to the SXPS probe are insignificant. The substrate surface between the clusters remains covered with a 1-ML Pt film as evidenced by the intensity and position of the surface Pt feature and the lack of W surface peaks at temperatures 1400–1700 K. The inset in Fig. 5 shows the intensity of W $4f$ features versus annealing temperature. The different phases of thermal evolution of the Pt/W(111) denoted on this graph have been assigned according to the above considerations.

B. Palladium

Due to the limited photon energy range of our apparatus (30–200 eV), the data for Pd/W could be obtained only in the $4f_{7/2}$ region of tungsten (the $3d$ levels of Pd are beyond the accessible photon energy range). A set of SXPS W $4f$ spectra for 1-ML Pd on W(111) recorded following annealing to increasingly higher temperatures is shown in Fig. 6. A shift of the W $4f_{7/2}$ peak corresponding to the faceting transition is visible at 800 K. The W surface peaks appear when the sample is annealed to temperatures at which Pd desorption from the Pd/W surface becomes efficient ($T > 1300$ K). The W $4f$ peak shift due to faceting is caused by a change of the Pd/W interface and Pd pseudomorphic film from (111) to (211) as illustrated in Figs. 7(a)–7(c). Annealing of the 1-ML film on W(211) does not cause a change in the W peak shape—the Pd/W(211) system does not undergo transformations upon annealing below Pd desorption temperatures [Fig. 7(a)]. The faceted Pd/W(111) and Pd/W(211) SXPS features are in fact identical, within experimental uncertainty, see Fig. 7(b). (The facet edges occupy little surface area and do not influence the SXPS spectra.) A direct comparison of the W $4f_{7/2}$ peaks for the planar and faceted Pd-covered W(111) surface is shown in Fig. 7(c). A more detailed analysis of W $4f$ peak shifts upon faceting can be found in Ref. 17.

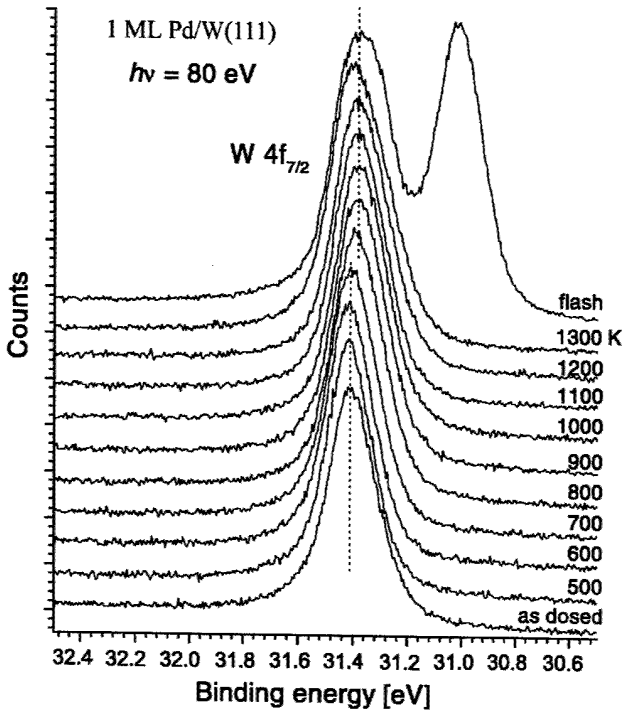

FIG. 6. W $4f_{7/2}$ SXPS spectra associated with annealing of a 1-ML Pd film on W(111).

Figure 8 shows W $4f$ peaks during growth of a multilayer Pd film on W(111). The dependence of the substrate peak height on Pd coverage is exponential (see inset in Fig. 8) indicating a flat form of growth. In contrast to Pt on W(111) (see Sec. III A 2 above), for Pd deposited on W(111) no satellite peaks have been observed in the W $4f$ region indicating no evidence of intermixing of Pd/W upon deposition.

For 10-ML coverage of Pd the W $4f$ substrate peaks are attenuated and scarcely visible (see in Fig. 9 the two lowest spectra in the sequence). Upon annealing, the film of Pd on W(111) undergoes complex changes. At annealing temperatures 450–500 K the substrate peaks increase in intensity, indicating that the layer is corrugated and the substrate areas

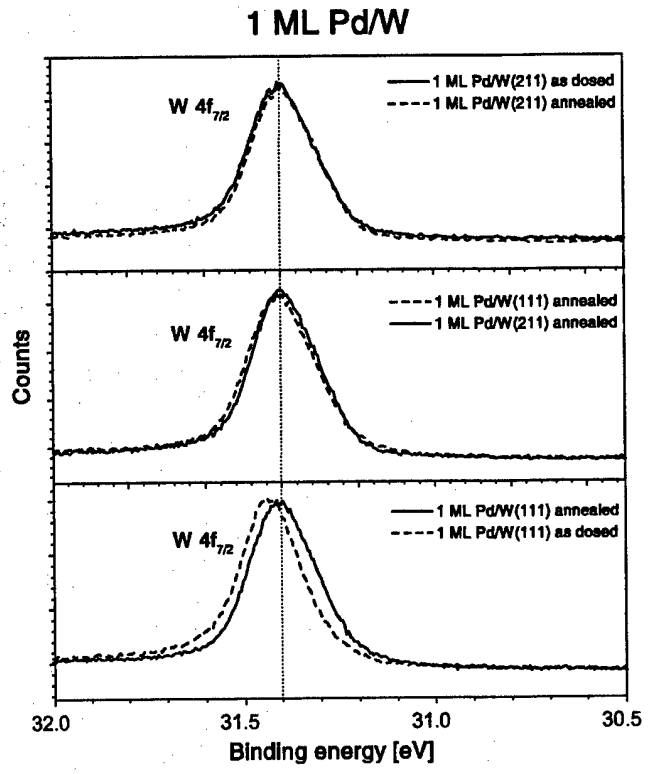

FIG. 7. A comparison of W $4f_{7/2}$ peaks for 1-ML Pd-covered W(211) and W(111).

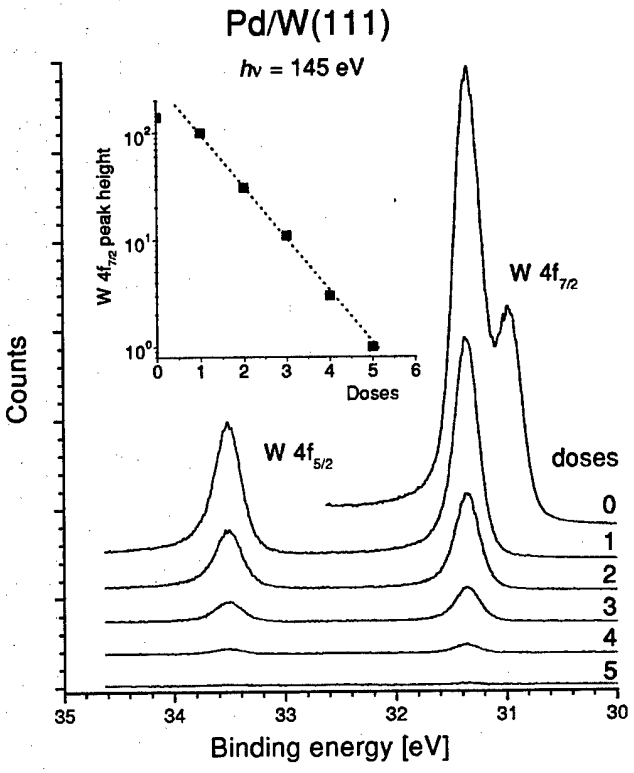

FIG. 8. W $4f$ spectra associated with growth of a multilayer Pd film on W(111) at room temperature. The inset shows the height of the W $4f_{7/2}$ peak as a function of coverage; one dose corresponds to ~1 ML.

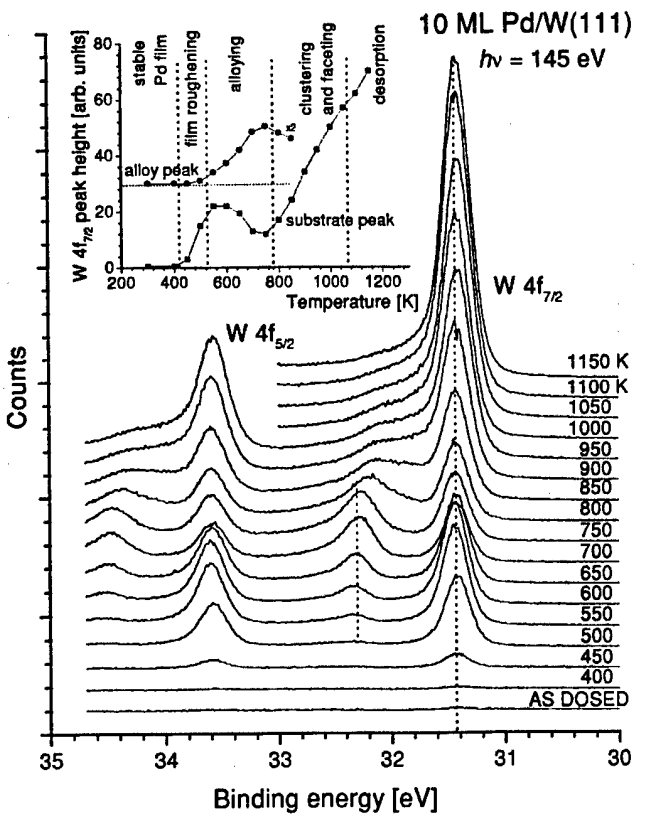

FIG. 9. W $4f_{7/2}$ SXPS spectra associated with annealing of a 10-ML Pd film on W(111). The inset shows the height of W $4f_{7/2}$ peaks as a function of annealing temperature.

covered with a thinner film are exposed. The dilute alloy peak appears at 550 K and increases up to 750 K. Simultaneously the substrate peak intensity is reduced back, reflecting increased attenuation of the W $4f$ peak by a corrugated alloy film (this may be an effect of the increasing alloy film volume due to incorporation of tungsten atoms into the film). Above 750 K the saturation of the alloy (evidenced by broadening of the alloy W $4f$ features) is accompanied by another substantial increase in the substrate peak intensity. At ~950 K, the intensity of the alloy peak decreases, evidencing the formation of relatively large three-dimensional clusters with small effective areas seen by x-ray photoelectron spectroscopy (XPS). [The threshold for thermal desorption of Pd from the Pd-W alloy formed by annealing is 1200 K (Ref. 2).] The W surface between clusters is covered with a 1-ML Pd film (no W $4f$ surface features are visible) and is faceted, as evidenced by the SXPS W peak position. The intensity of the substrate W $4f$ features vs annealing temperature is plotted in the inset in Fig. 9. The evolution phases of the Pd/W(111) system are denoted on this graph.

C. Iridium

The $4f$ SXPS spectra associated with the growth of multilayer Ir on W(111) are shown in Figs. 10 and 11. Previously it has been found for Ir/W(211) that Ir SXPS $4f$ peaks are not shifted if the Ir neighbor atom is exchanged by a W atom.[4] Such stability of the Ir atom electronic structure

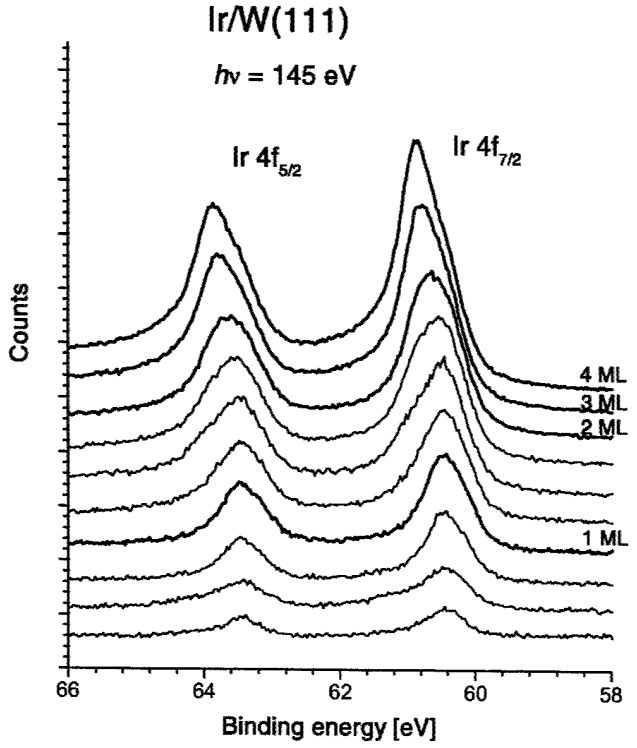

FIG. 10. An Ir $4f$ spectral region recorded during growth of an Ir film on W(111) at 300 K.

is also evident for the Ir/W(111) system, see Fig. 10, where in contrast to Pt/W(111), there is little variation of the Ir peak shape in the submonolayer coverage regime. The feature is clearly multicomponent but the different lines are due to atoms with different coordination numbers rather than due to atoms at the interface experiencing different chemical interactions with the substrate (which was the case for Pt/W). At 4 ML the "surface" shoulder on the low BE side is much less intense than for Ir/W(211) indicating that it may be associated with the top geometrical layer rather than with a top physical layer [which was the case for W(211)-based systems].

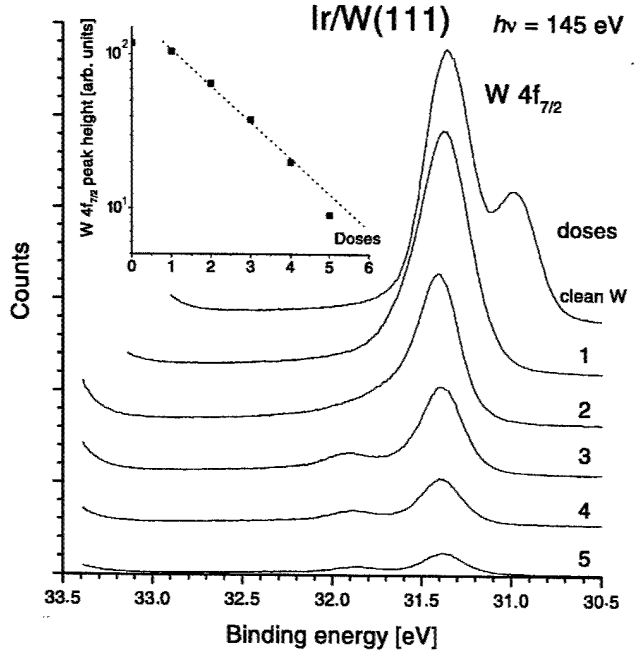

FIG. 11. W $4f$ spectra associated with growth of a multilayer Ir film on W(111) at room temperature. The inset shows the height of the W $4f_{7/2}$ peak as a function of coverage; one dose corresponds to ~1-ML coverage.

The dependence of the substrate XPS peak intensity on the film thickness is exponential, see the inset in Fig. 11. This indicates that the growth proceeds in a flat mode. (The small deviation of experimental data from the straight line in Fig. 11 is assigned to increase in deposition rate arising from gradual thinning of the Ir wire which is the source of Ir atoms.) For coverages greater than 2 ML additional peaks appear in the W $4f$ region evidencing an interface mixing similar to the one observed for Pt/W(111) (Sec. III A). These peaks are shifted by 0.5 eV to higher BE, and we assign these peaks to a W impurity in an Ir host (or dilute W in an Ir alloy, cf. Ref. 4).

The annealing sequence for 1 ML of Ir/W(111) is presented in Fig. 12. At different phases of annealing the W $4f$ spectra show rather complex behavior. As shown by LEED the "as-dosed" film surface has a $(2\sqrt{3}\times 2\sqrt{3})R30°$ structure and the SXPS Ir $4f_{7/2}$ feature displays a shoulder on the high binding-energy side of the SXPS peak. Upon heating to 500 K the LEED pattern changes to $(\sqrt{3}\times\sqrt{3})R30°$ and a shoulder appears on the high BE side of the W $4f$ feature. Above 800 K the W $4f_{7/2}$ peak becomes single-component and the LEED pattern changes indicating a faceting of the Ir film covered surface to (211). Upon further heating LEED shows coexistence of faceted and $(\sqrt{3}\times\sqrt{3})R30°$ reconstructed regions. The shoulder on the high BE side of the Ir peak reappears and the $4f$ feature resembles closely that before the faceting transition. These observations indicate that the surface has been converted partially to a planar one. Above 2100 K the monolayer desorption threshold is reached and the surface W $4f$ components are finally seen on the low BE side (Fig. 12).

In Fig. 13 an annealing sequence for ~7 ML of Ir on W(111) is shown. Dilute alloy peaks are present in the W $4f$ region for annealing temperatures up to 1000 K. Within this temperature range Ir $4f$ peaks show little variation. Above 1100 K the W $4f$ alloy peaks shift to lower BE and broaden indicating the formation of a saturated alloy film. At 1000 K the Ir $4f$ features change; the bulk Ir peak decreases in height, which reflects the decreased content of Ir in the bulk of the film. Within the range 1300–1700 K the system does not undergo further transformations as evidenced by constant SXPS shapes and intensities. This is illustrated in the inset in Fig. 13. Around 2000 K the Ir bulk alloy $4f$ components disappear as a result of thermal desorption of the Ir-W alloy.

D. Rhodium

For rhodium (a $3d$ metal), the data are limited to the $4f$ levels of the W substrate. During the growth of Rh films on W(111) the attenuation of substrate W $4f$ features is exponential as a function of coverage, evidencing a flat form of

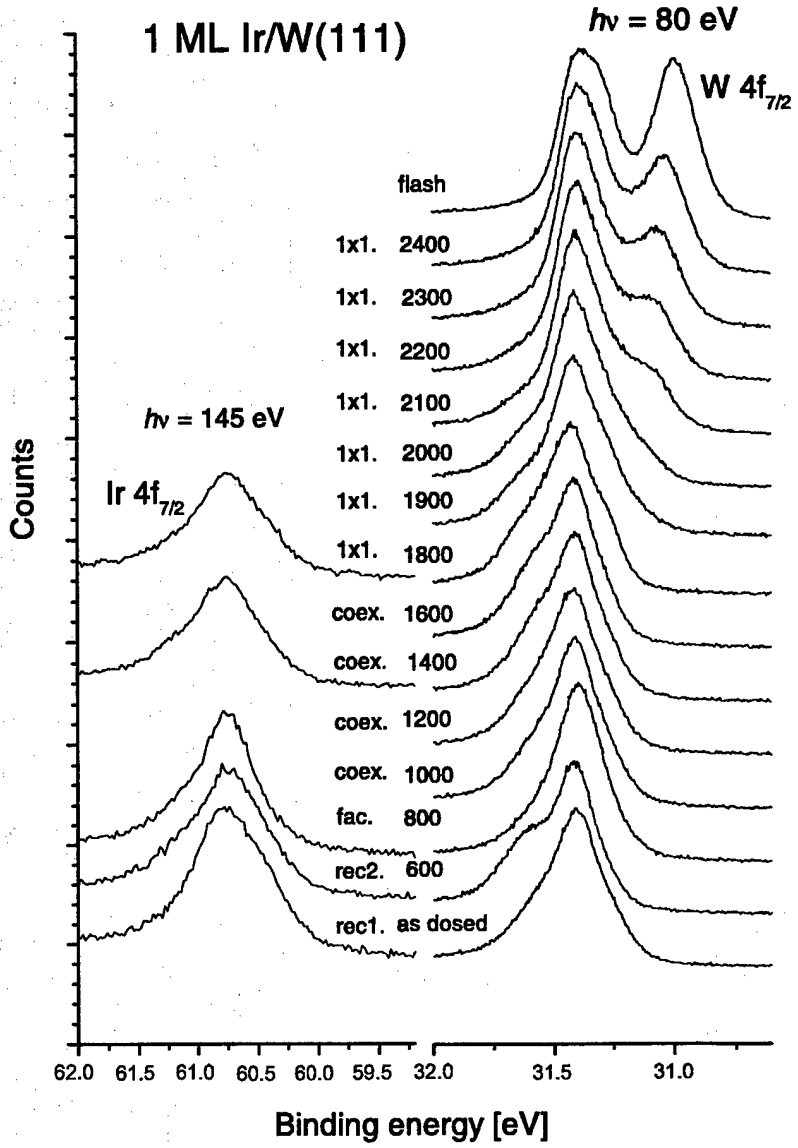

FIG. 12. Ir $4f_{7/2}$ and W $4f_{7/2}$ SXPS spectra associated with the annealing sequence for a 1-ML Ir film on W(211). Annealing time is 1 min. The meanings of the reconstruction labels are the following: "rec1.," $(2\sqrt{3}\times 2\sqrt{3})R30°$, "rec2.," $(\sqrt{3}\times\sqrt{3})R30°$, "fac.," faceted, and "coex.," coexistence of faceted and "rec2."

growth of Rh on W(111), see the inset in Fig. 14. For coverages higher than 1 ML additional peaks characteristic of a Rh impurity in the W host appear (see Fig. 14) shifted by ~0.5 eV to higher BE indicating adsorption-triggered interface mixing similar to that observed for Pt and Ir/W(111) (discussed in Secs. III A and III C).

An annealing sequence for ~8 ML of Rh on W(111) is shown in Fig. 15. The as-dosed spectrum show peaks due to the attenuated W substrate and dilute W in Rh. Above 500 K the two peaks increase concurrently. Above 650 K the dilute alloy Rh peak increases further while the substrate peak decreases, similar to Pd/W(111) (Sec. III B). The dilute Rh-W phase exists below an annealing temperature of 850 K. At 900 K the alloy peak broadens and shifts to lower binding energy. Simultaneously the substrate peak increases its intensity. Above 1000 K the alloy-related feature is almost invisible suggesting that the alloy forms large three-dimensional clusters. Around 2000 K the W surface peaks appear as a result of thermal desorption of Rh from the surface.

IV. DISCUSSION

A. Single monolayer films on W(111)

In general the deposition of metal on metal at room temperature leads to a metastable configuration. This configuration reflects the kinetics of deposition, diffusion, and growth processes, and the existence of diffusion (reaction) barriers.[7] This metastable state can survive in a limited temperature range. Annealing causes the energetic barriers to be overcome and the system lowers its free energy through intermixing and modification of the surface structure. Finally if the annealing temperature/time is sufficient the system may approach the global energy minimum.

Bimetallics involving transition metals are often extremely complex and synchrotron-radiation-based soft-x-ray photoelectron spectroscopy is a technique of choice for studying these systems. However, recent advances in accurate first-principles computational techniques have made it possible to calculate reliable segregation energies for a large number of close-packed transition-metal alloy surfaces.[11]

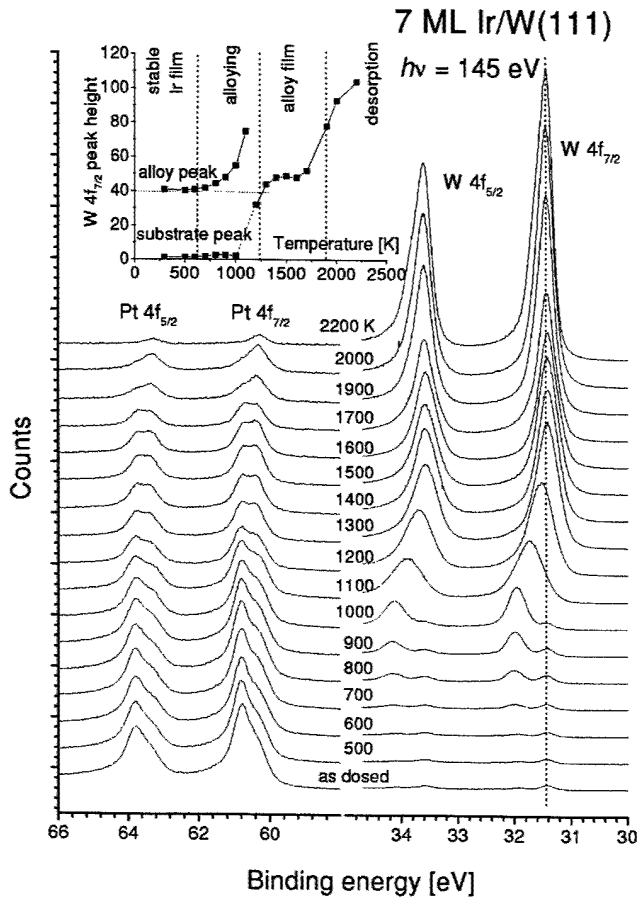

FIG. 13. Ir $4f$ and W $4f$ SXPS spectra associated with the annealing sequence for a 7-ML Ir film on W(111). Annealing time is 1 min.

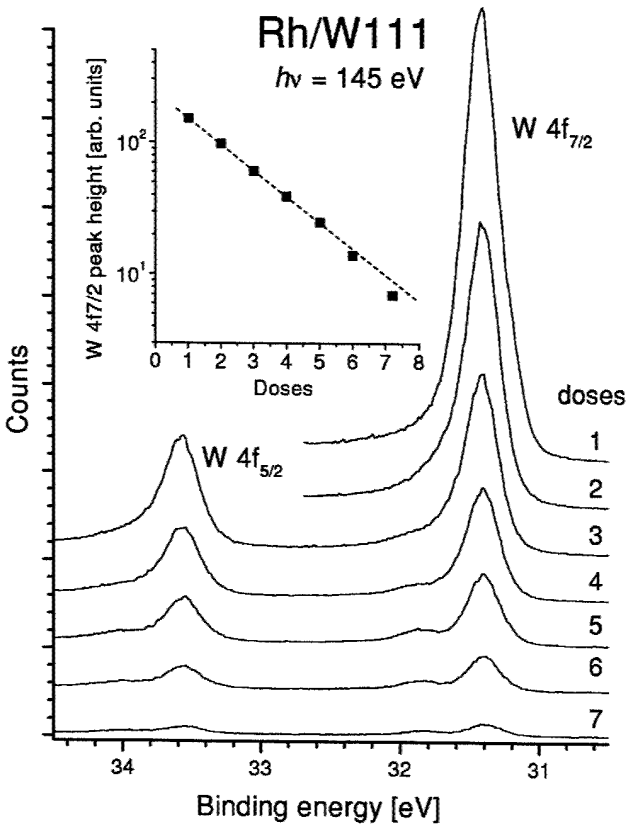

FIG. 14. W $4f$ spectra associated with the growth of a multilayer Rh film on W(111) at room temperature. Inset shows the height of the W $4f_{7/2}$ peak as a function of coverage; one dose corresponds to ~1 ML.

Such complete data arrays are extremely helpful in understanding and analyzing experimental data.

During annealing, if the segregation energy is negative, a metastable film of metal on a metal substrate will eventually dissolve into the bulk. If the segregation energy is positive, the metal tends to stay in the surface layer. However, the entropy factor in the free energy always favors an intermixed system and due to this factor at temperatures high enough to overcome diffusion barriers, the deposit may be slowly lost into the bulk.

Segregation energies for transition metals on the close-packed (110) surface of W have been calculated by Ruban *et al.*[11] Although in extreme cases the surface segregation energy may reverse its sign depending on the crystal face (for example, the PtNi alloy[19]) usually it is reasonably well described by a bond breaking model, from which it is assessed that the segregation energies scale by a factor up to 1.7 going from close-packed to open surfaces.[20] Based on the calculation of Christensen *et al.*,[7] it is expected that all metals reported here strongly segregate from a W host on both (211) and (111) crystal faces. This is indeed seen in our experimental data; a single physical monolayer of deposited metal (Pt, Pd, Ir, Rh) tends to remains on top of W(111). These findings are also consistent with previous data obtained by low-energy ion scattering,[21] and Auger electron spectroscopy (AES).[14,15] Similar segregation phenomena have been seen on W(211) with our previous SXPS studies.[4] For 1-ML Ir on W(111) annealed to $T=600$ K the change in the LEED pattern and the additional shoulder in the W $4f$ spectrum indicate formation of an ordered surface alloy phase.

Planar W(111) covered with 1 ML of Pt, Pd, Ir, and Rh is unstable upon heating, and a massive reconstruction occurs if the surface is heated above 700 K. As a result the surface is covered with pyramidal facets exposing {211}-type planes.[1] Following this transformation a monolayer of deposited metal still "floats" on the substrate.

For W covered with a single-monolayer metal film its W $4f$ SXPS peaks are composed of bulk and interface components. As a result of the faceting reconstruction the interface is converted from a (111) to (211) type, and the interface component of the SXPS features changes. This change is most apparent for the Pd/W system; for other systems studied the change is small (see also Ref. 17). An effect of faceting is also visible in the changing shape of overlayer metal (Pt and Ir) $4f$ SXPS peaks; faceted surfaces which expose {211} planes covered by 1-ML films produce single-component $4f$ features, as opposed to planar (111) surfaces which produce $4f$ features that cannot be described by single DS line shapes.

As evidenced by LEED, ultrathin late-transition-metal films on W(111) grown at room temperature are pseudomor-

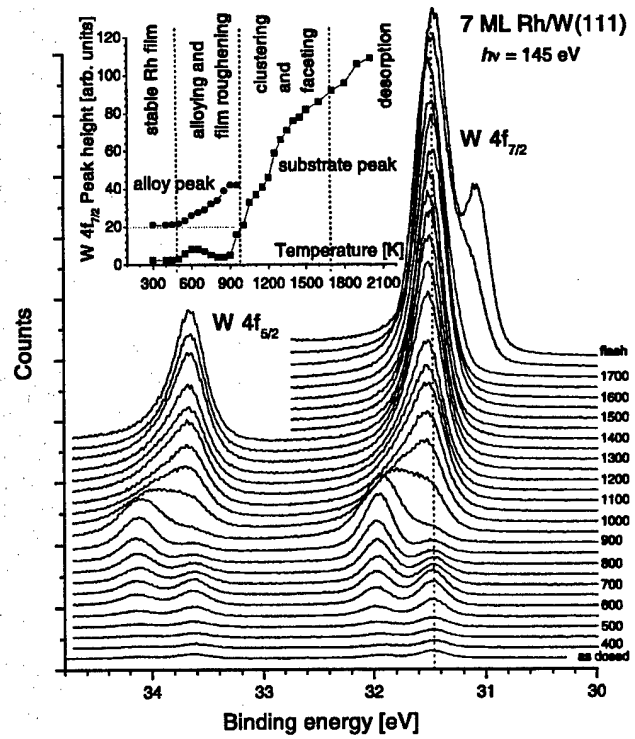

FIG. 15. W $4f_{7/2}$ SXPS spectra associated with the annealing sequence for a ~7-ML Rh film on W(111). Inset shows the substrate and dilute alloy W $4f_{7/2}$ peak intensity vs coverage.

phic. Results obtained for Pt/W(111) indicate that for coverages less than a single physical monolayer the growth has a well-defined layer-by-layer character. Distinct SXPS peaks for different geometrical "monolayers" in the pseudomorphic (111) bcc layer indicate that each lower layer is completed before the next one starts to grow. This is an important observation which helps in understanding the faceting surface phase transition. As shown in Ref. 22 the driving force for the transition is a surface energy difference between film covered W(111) and W(211) surfaces. The critical coverage for faceting to occur is 1 ML. Locally the coverage may reach 1 ML (in $2d$ islands) if the average coverage exceeds 2/3 ML. Such faceted 2d islands on a W(111) surface have been indeed revealed in recent LEEM and scanning tunneling microscopy (STM) studies.[23,24] In the present work the faceting transition has been observed on fully covered W(111) surfaces for annealing temperatures greater than 700 K for Pt, Pd, and Ir films. Interestingly the Pd-covered faceted surface is the most stable. Annealing the Pd-covered faceted W(111) surface causes an increase in the facet size but the overall character of the surface does not change. In contrast Pt- and Ir-covered faceted surfaces undergo further transformations upon annealing to temperatures ~1000 K; the surface is partially converted back to a planar one. This is evidenced by LEED patterns and by Pt and Ir $4f$ SXPS peak shapes. For the Pt/W system STM images of partially faceted and partially planar surfaces have been also published.[14] This phenomenon is likely to be associated with the decreasing amount of the overlayer material at the surface. Since the loss of facets occurs below the desorption threshold of Pt or Ir from W, the reason behind this could be the diffusion of Pt (or Ir) into the bulk driven by the entropy factor in the free energy. It may be deduced from binary-alloy phase diagrams[25,26] that each of the metals studied in this work has low solubility in a tungsten matrix, however, the solubility of Pt and Ir is significantly higher than that of Pd.

B. Multilayer films on W(111)

Previous studies of multilayer Pt film growth on W(111) by AES and LEED (Ref. 14) indicated that the growth is pseudomorphic, but not in a perfect layer-by-layer mode. In the present experiment this is confirmed for all four admetals studied since the attenuation of the substrate feature during growth is exponential and the LEED pattern remains (1 ×1) during growth but its sharpness deteriorates with increasing coverage. We conclude that the overlayers studied fully cover the substrate although their surfaces are not atomically flat. The growth proceeds in a random mode (similar to a "sticks-where-it-hits" mode). The $4f$ SXPS features (Pt and Ir) originating from multilayer films include the bulk feature and several components associated with different geometrical monolayers at the surface and at the interface. These multiple components appear at slightly different positions; their superposition forms a smooth curve which cannot be decomposed uniquely.

An interesting property of Pt, Rh, and Ir on W(111) is the mixing at the interface observed during deposition of overlayers at room temperature. Although the Pd/W system is chemically similar to the other systems studied, interface mixing does not occur for this case. In no case does the intermixing occur when the coverage is less than 1 ML. At 2–3-ML coverage the "intermixed" W peak is already clearly visible. The position of the peak corresponds to dilute W in a Pt (Ir, Rh) host. As indicated by the intensity of the "intermixed" peak, relative to the substrate peak, the mixing stops at 6–7-ML coverage. A very interesting aspect of this observation is that the adsorption of a metal atom at the film surface can trigger the site exchange process at a remote interface.

Recently Sprague and Gilmore[27] have shown by molecular-dynamics simulations that inelastic processess initiated by an atom impact on the surface can lead to interface mixing. In particular for Pt deposited on a Cu substrate a mixing has been found for thermal Pt energies. Interface mixing caused by electronic excitation has been reported also for a NiTi interface bombarded by GeV heavy ions.[28] It has been concluded that the mixing is caused by a short-lived lattice excitation in the immediate vicinity of an atom impact. The W/Pt (Ir, Rh) interface mixing observed in the course of our experiments can be described by similar words, although the exact nature of the phenomenon is not yet clear. The energetic barriers for intermixing are similar at all four interfaces studied (as indicated by similar thermal thresholds for mixing ~600 K, see the discussion below). The process is clearly driven by a release of energy upon adsorption of a metal atom on the film surface. Cohesive energies of metals studied have been compared in Table I. The energy for Pd is considerably smaller than for other metals and the presence of intermixing may be correlated with the value of the cohesive energy.

TABLE I. Relationship between cohesive energies and interface mixing during deposition of overlayers on a W substrate at 300 K.

Metal	Cohesive energy (eV/atom)	Mixing
Ir	6.95	yes
Pt	5.85	yes
Rh	5.76	yes
Pd	3.9	no

An interface between two metals formed at room temperature is typically metastable since interface diffusion barriers hinder intermixing. However, the mixing is likely to occur during annealing. In general there are several possibilities: e.g., for an A/B interface, A and B may preferentially remain in separate phases, or they may mix mutually, or A preferentially diffuses into B, or vice versa. In particular, if the deposited metal diffuses (dissolves) in the substrate, an ultrathin film of such a metal would, upon annealing, disappear from the surface, forming a dilute alloy with the substrate. However, if the deposited metal is not allowed to diffuse into the substrate it may stay on the surface as is, or form clusters, a surface alloy, or alloy clusters. Relevant examples, as seen by SXPS, have been demonstrated in our previous paper[4] for Pt, Pd, Ir, Rh, and Au on W(211). Films of Pt, Pd, Ir, or Rh on W(211) are transformed into flat alloy films upon annealing; a dilute alloy phase is observed below 900 K for Pt and Pd and below 1400 K for Ir and Rh. For higher annealing temperatures ($T>1400$ K) saturated alloy films are formed. Following SXPS peak assignments from Ref. 4 we are able to analyze the thermal evolution for more complex W(111)-based bimetallic systems. Ir on W(111) resembles closely Ir/W(211); initially a dilute W in the Ir alloy film is formed (600–1000 K). Above 1200 K a film of a saturated Ir-W alloy covers the W substrate.

Phenomena induced by heating Pt, Pd, and Rh films on W(111) are more diverse. Pt on W(111) resembles Pt on W(211) only during the dilute alloy phase at 600–900 K. In the case of Pd on W substantial corrugation of the film occurs before a dilute alloy is formed. For Rh films dilute alloy formation and initial film corrugation occur simultaneously. Since W atoms preferentially diffuse into Pt, Pd, and Rh the alloying process continues after formation of clusters. A common feature resulting from strong segregation trends (see Sec. IV A) is observed for all systems studied; a monolayer of late-transition metal always covers the tungsten substrate between clusters. Despite their chemical similarity, Ir, Pt, Pd, and Rh multilayer films exhibit different detailed behavior during annealing. The complexity in the electronic structure of transition-bimetallic systems means that the detailed structure and thermal transformations of a particular system cannot be predicted in a simple way. As discussed in Ref. 4 the observed SXPS peak shifts have no transparent relationship to alloy chemistry since the photoelectron peak shifts for transition metals are influenced by several competing effects; initial-state charge transfer tends to be rather small as the localized d orbital charge transfer is compensated for by a free s-, p-like charge. Other effects include final-state screening changes, intra-atomic shifts in valence level populations (rehybridization), or reference level changes.[29] The interplay of these many subtle effects is also impossible to predict in a simple way. Despite these difficulties, based on relative intensities of SXPS peaks, their order of appearance during growth, and their annealing behavior, it is possible to identify the chemical configuration of atoms emitting photoelectrons in particular SXPS lines and to successfully investigate the structure and transformations of the bimetallic system.

V. CONCLUSIONS

Several late-transition metals (Pt, Pd, Ir, Rh) grow in layers on W(111). The films have pseudomorphic structure for the initial few monolayers. A single monolayer of these metals on W(111) remains on the surface upon annealing, which is attributed to strong segregation trends of late-transition metals on W surfaces. The W(111) substrate covered with a single-monolayer film of a late-transition metal (Pt, Pd, Ir, Rh) and annealed is faceted to W(211). During growth of multilayer films of Pt, Ir, and Rh at room temperature, adsorption processess at the surface lead to mixing at the remote interface. Upon annealing, multilayer films of Pt, Pd, Ir, and Rh undergo complex transformations including alloying, segregation, clustering, and faceting of the surface between clusters. Although there are common features observed in the thermal evolution of these bimetallic systems, the detailed transformations are system-specific.

ACKNOWLEDGMENTS

This work has been supported in part by the U.S. Department of Energy, Office of Basic Energy Sciences and by the U.S. Army Research Office.

*Present address: Instytut Fizyki, Uniwersytet Jagiellonski, Reymonta 4, 30-059 Krakow, Poland.
†Corresponding author.

[1] T.E. Madey, J. Guan, C.-H. Nien, C.-Z. Dong, H.-S. Tao, and R.A. Campbell, Surf. Rev. Lett. **3**, 1315 (1996).
[2] T.E. Madey, C.-H. Nien, K. Pelhos, J.J. Kolodziej, I.M. Abdelrehim, and H.-S. Tao, Surf. Sci. **438**, 191 (1999).
[3] J.J. Kolodziej, K. Pelhos, I.M. Abdelrehim, J.W. Keister, J.E. Rowe, and T.E. Madey, Prog. Surf. Sci. **59**, 117 (1999).
[4] J.J. Kolodziej, T.E. Madey, J.W. Keister, and J.E. Rowe, Phys. Rev. B **62**, 5150 (2000).
[5] G.A. Attard and D.A. King, Surf. Sci. **222**, 360 (1989).
[6] R.W. Judd, M.A. Reichelt, E.G. Scott, and R.M. Lambert, Surf. Sci. **185**, 515 (1987).
[7] A. Christensen, A.V. Ruban, P. Stoltze, K.W. Jacobsen, H.L. Skriver, and J.K. Norskov, Phys. Rev. B **56**, 5822 (1997).
[8] J.G. Che, C.T. Chan, C.H. Kuo, and T.C. Leung, Phys. Rev. Lett. **79**, 4230 (1997).
[9] A.M.N. Niklasson, I.A. Abrikosov, and B. Johansson, Phys. Rev. B **58**, 3613 (1998).
[10] D. Wu, W.K. Lau, Z.Q. He, Y.J. Feng, M.S. Altman, and C.T. Chan, Phys. Rev. B **62**, 8366 (2000).

[11] A.V. Ruban, H.L. Skriver, and J.K. Norskov, Phys. Rev. B **59**, 15 990 (1999).
[12] P. Thiry, P.A. Bennett, S.D. Kevan, W.A. Royer, E.E. Chaban, J.E. Rowe, and N.V. Smith, Nucl. Instrum. Methods Phys. Res. A **222**, 85 (1984).
[13] W. Xu and J.B. Adams, Surf. Sci. **319**, 45 (1994).
[14] C.Z. Dong, S.M. Shivaprasad, K.-J. Song, and T.E. Madey, J. Chem. Phys. **99**, 9172 (1993).
[15] K.-J Song, C.-Z Dong, and T.E. Madey, Langmuir **7**, 3019 (1991).
[16] H.-S Tao, J.E. Rowe, and T.E. Madey, Surf. Sci. **407**, L640 (1998).
[17] H.-S Tao, C.-H. Nien, T.E. Madey, J.E. Rowe, and G.K. Wertheim, Surf. Sci. **357**, 55 (1996).
[18] K. Pelhos, Ph.D. thesis, Rutgers University, 1999.
[19] I.A. Abrikosov, A.V. Ruban, H.L. Skriver, and B. Johansson, Phys. Rev. B **50**, 2039 (1994).
[20] A.V. Ruban and H.L. Skriver, Comput. Mater. Sci. **15**, 119 (1999).
[21] C.Z. Dong, L. Zhang, U. Diebold, and T.E. Madey, Surf. Sci. **322**, 221 (1995).
[22] J.G. Che, C.T. Chan, C.H. Kuo, and T.C. Leung, Phys. Rev. Lett. **79**, 4230 (1997).
[23] K. Pelhos, J.B. Hannon, G.L. Kellogg, and T.E. Madey, Surf. Sci. **432**, 115 (1999).
[24] K. Pelhos, T.E. Madey, J.B. Hannon, and G.L. Kellogg, Surf. Rev. Lett. **5**, 767 (1999).
[25] F.A. Shunk and M. Hansen, *Constitution of Binary Alloys, 2nd Supplement* (McGraw-Hill, New York, 1969).
[26] R.P. Elliot and M. Hansen, *Constitution of Binary Alloys, 1st Supplement*, (McGraw-Hill, New York, 1965).
[27] J.A. Sprague and C.M. Gilmore, Thin Solid Films **272**, 244 (1996).
[28] R. Leguay, A. Dunlop, F. Dunstetter, N. Lorenzelli, A. Braslau, F. Bridou, J. Corno, B. Pardo, J. Chevallier, C. Colliex, A. Menelle, J.L. Rouviere, and L. Thome, Nucl. Instrum. Methods Phys. Res. B **122**, 481 (1997).
[29] R.E. Watson and M.L. Perlman, Phys. Scr. **21**, 527 (1980).

Nanoscale surface chemistry

Theodore E. Madey*†, Kalman Pelhos*, Qifei Wu‡, Robin Barnes*, Ivan Ermanoski*, Wenhua Chen*, Jacek J. Kolodziej*, and John E. Rowe§

*Department of Physics and Astronomy and Laboratory for Surface Modification, and ‡Department of Chemistry, Rutgers, The State University of New Jersey, Piscataway, NJ 08854-8019; and §United States Army Research Office, PO Box 12211, Research Triangle Park, NC 27709-2211

Edited by Robert Gomer, The University of Chicago, Chicago, IL, and approved January 9, 2002 (received for review October 10, 2001)

We report evidence in several experiments for nanometer-size effects in surface chemistry. The evidence concerns bimetallic systems, monolayer films of Pt or Pd on W(111) surfaces. Pyramidal facets with {211} faces are formed on annealing on physical monolayer of Pt, Pd on a W(111) substrate, and facet sizes increase with annealing temperature. We used synchrotron radiation-based soft x-ray photoemission to show that monolayer films of Pt, Pd, on W "float" on the outer surface, whereas multilayer films form alloys on annealing. Acetylene reactions over bimetallic planar and faceted Pd/W surfaces exhibit size effects on the nanometer scale, that is, thermal desorption spectra of reactively formed benzene and ethylene (after acetylene adsorption) change systematically with facet size. In the second case, the decomposition of C_2H_2 over planar and faceted Ir(210) surfaces also exhibits structure sensitivity; temperature programmed desorption of H_2 from C_2H_2 dissociation depends on the nanoscale surface structure. Finally, we have characterized interactions of Cu with the highly ordered S(4 × 4)/W(111) surface. The substrate is a sulfur-induced nanoscale reconstruction of W(111) with (4 × 4) periodicity, having broad planar terraces (≈30 nm in width). Fractional monolayers of vapor-deposited Cu grow as threedimensional clusters on the S(4 × 4) surface over a wide coverage range. At low Cu coverage (≤ 0.1 ML), Cu nanoclusters nucleate preferentially at characteristic 3-fold hollow sites; we find a clear energetic preference for one type of site over others, and evidence for self-limiting growth of nanoclusters.

An important issue in surface chemistry and catalysis is how surface structures and features with nanometer dimensions affect reactivity in heterogeneous systems (1–3). The focus of our work has been on several aspects of nanoscale phenomena that influence surface chemistry, including faceting of metallic and model bimetallic catalyst surfaces, and nucleation of subnanometer metallic clusters on sulfided surfaces. We study atomically rough substrates [bcc (111) surface of W, and fcc (210) surface of Ir] that are morphologically unstable, that is, the initially planar substrate becomes covered with nanoscale facets when covered with monolayer films of gases or other metals, and heated to elevated temperature. Major objectives of this work have been (*i*) to determine how the surface transition from planar to faceted affects the surface reactivity of metallic and bimetallic systems, and (*ii*) to characterize the nucleation and growth of metals on sulfided W surfaces. The three main components of this effort are surface structure, surface chemistry, and surface electronic properties.

The importance of bimetallic catalysts based on Pt-group metals has been increasing in recent decades (4, 5). These catalysts display important advantages over classical reforming catalysts, including better stability, as well as improved activity and selectivity. In particular, refractory metals (W, Mo, Re, . . .) in combination with Pt-group metals are active catalysts for hydrogenation and hydrogenolysis reactions (6–9).

Our previous work in the area of bimetallic surfaces is summarized in two review articles (10, 11). In brief, morphologically unstable W(111) and Mo(111) coated with a single physical monolayer (ML) of certain metals or other elements (Pd, Rh, Ir, Pt, Au, O) undergo massive reconstruction from a planar morphology to a microscopically faceted surface on heating to $T > 700$ K. Three-sided nanometer-sized pyramids form in which the facet sides are mainly film-covered {112} facets. The faceting transition in these systems is believed to be thermodynamically driven but kinetically limited: annealing is needed to achieve sufficient surface atom mobility for mass transport. The overlayer film increases the anisotropy in surface free-energy and enhances the relative stability of the faceted morphology. Striking evidence for structure sensitivity is seen in catalytic hydrogenolysis of butane over planar and faceted Pt/W. Recent synchrotron radiation studies using soft x-ray photoemission spectroscopy (SXPS) have provided insights into the electronic properties and thermal stability of the bimetallic systems.

In the following paragraphs, we describe recent results and focus on three main aspects of the studies: surface structure and morphology, surface chemistry, and surface electronic properties. We begin with atomistic studies of faceting and reconstruction in bimetallic systems based on W(111) and discuss evidence that acetylene reactions over Pd/W(111) surfaces exhibit size effects on the nanometer scale. We use SXPS to show that interfacial mixing, even at 300 K, is observed for multilayers of Pt, Rh, Ir on W(111), whereas monolayer films are stable at high T. We report the oxygen-induced faceting of Ir(210), and describe structure sensitivity in C_2H_2 chemistry over clean planar and clean faceted Ir(210). We describe studies of metals on sulfided W(111), including self-limiting growth of Cu nanoclusters on specific surface sites.

This program includes detailed microscopic studies of faceting of metal substrates induced by monolayer overlayer films. We believe the results of these studies are important in understanding the mechanisms of possible dynamic structural rearrangements at the surfaces of high area metallic and bimetallic catalysts under high-temperature operation.

Methods

In this work we have used an array of ultrahigh vacuum surface science methods, including high-resolution scanning tunneling microscopy (STM), low energy electron diffraction (LEED), and

This paper results from the Arthur M. Sackler Colloquium of the National Academy of Sciences, "Nanoscience: Underlying Physical Concepts and Phenomena," held May 18–20, 2001, at the National Academy of Sciences in Washington, DC.

This paper was submitted directly (Track II) to the PNAS office.

Abbreviations: ML, monolayer; TPD, temperature programmed desorption; STM, scanning tunneling microscopy; LEED, low-energy electron diffraction; LEEM, low-energy electron microscopy; SXPS, soft x-ray photoemission spectroscopy; HRSXPS, high-resolution SXPS; L, Langmuir.

†To whom reprint requests should be addressed. E-mail: madey@physics.rutgers.edu.

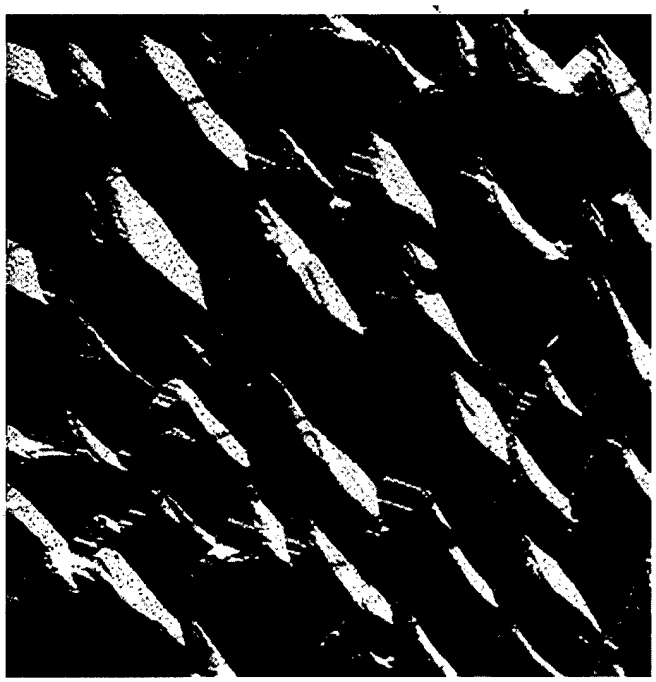

Fig. 1. STM image of fully faceted W(111) surface: Pt coverage is ≈1.1 physical ML, annealed at 1,200 K for 1 min. Field of view is 2,000 Å × 2,000 Å. Sample bias: +1.5 V, tunneling current: 1.5 nA. STM images of Figs. 1 and 2 are displayed in XSLOPE mode, which gives a three-dimensional top view perspective of the pyramids with {211} facets. [Reproduced with permission from ref. 13 (Copyright 1999, World Scientific).]

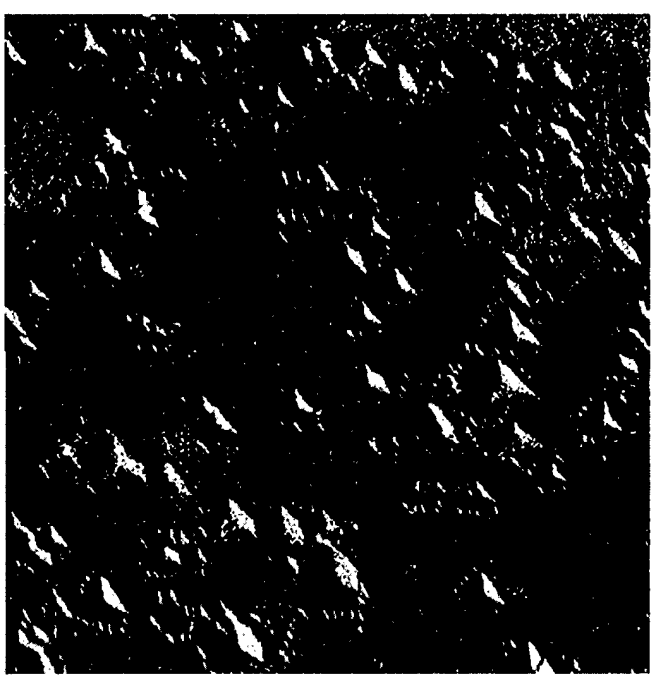

Fig. 2. STM image (5,000 Å × 5,000 Å) of a partially faceted surface. Pt coverage is ≈0.8 physical ML, annealed at 1200 K for 1 min. Relatively large pyramids (200–700 Å in size) are scattered on the otherwise smooth planar surface, sometimes standing individually, sometimes forming large clusters that are several thousand Angstroms in extent. [Reproduced with permission from ref. 13 (Copyright 1999, World Scientific).]

low-energy electron microscopy (LEEM) for structure and morphology; temperature-programmed desorption (TPD) for surface chemistry; and high-resolution SXPS (HRSXPS) using synchrotron radiation for electronic properties.

Results and Discussion

Faceting of W(111) Induced by Ultrathin Metal Films. We have used two microscopic methods to provide insights into the mechanism of metal film-induced faceting of bcc(111) surfaces, and have found evidence for the nucleation and growth of faceted regions (12, 13). LEEM and STM have been used to investigate the faceting of W(111) as induced by Pt. The atomically rough W(111) surface, when fully covered with a monolayer film of Pt and annealed to temperatures higher than ≈750 K, experiences a significant morphological restructuring: the initially planar surface undergoes a faceting transition and forms three-sided pyramids with {211} faces as seen clearly in the STM image of Fig. 1. In complementary studies, LEEM can distinguish between planar and faceted surfaces based on the different types of diffraction of low-energy electrons on surfaces with different morphologies, with up to ≈70-Å lateral resolution. LEEM measurements (12, 13) of Pt/W(111) demonstrate that the transition from planar to faceted structure proceeds through the nucleation and growth of spatially separated faceted regions. The surface remains planar for Pt coverages less than ⅔ ML (1 ML = 1.7×10^{15} atoms per cm^2). As the Pt coverage increases above ⅔ ML on the heated W surface, local islands of Pt with coverage of 1 ML are able to nucleate, and it is there that facets form. When the entire surface has a coverage of 1 ML, the surface is fully faceted.

STM data (Fig. 2) confirm the LEEM observations that a partially faceted Pt/W surface is a combination of large planar regions with scattered faceted regions. The faceted regions include pyramids of two distinct size distributions (Fig. 2): large individual pyramids or clusters of large pyramids, surrounded by smaller size satellite pyramids. LEEM and STM prove to be excellent complementary microscopic techniques in the study of faceting. STM provides structural information down to atomic scale. Although the resolution of LEEM does not match that of an STM, LEEM has several advantages that make it a most useful tool in studying the kinetics of large scale morphological transformations: it is capable of imaging surfaces at very high temperatures, and the surface is easily observed during metal deposition.

There is ample documentation that the atomically rough W(111) surface develops nanometer-scale facets with W{211} orientation when covered by 1 ML films of Pd, Pt, Rh, or Ir, followed by annealing (10, 11). In recent experiments, we have found that the metal film-covered W(211) surface itself may undergo a faceting transition (14). A W(211) surface covered with a thin film (between 0.5 and 1 physical monolayer) of Rh, Pt or Pd is found to exhibit an $n \times 1$ superstructure when annealed above a threshold temperature of ≈900 K (500 K for Pd). The superstructure is observed by using low-energy electron diffraction: phase diagrams have been measured to indicate the coverage range and the temperature threshold where the new structure appears. Scanning tunneling microscopy results indicate that in the case of Pd/W(211) the superstructure phase is caused by missing overlayer rows (Fig. 3), but in the case of Rh/W(211) it is more likely caused by a microfaceting of the surface into {110} faces (14). Overlayer coverages >1 ML are thermally unstable, and form ultrathin alloy films on annealing. Alloy formation for thermally annealed multilayers of Rh, Pd, Pt on W(211) is confirmed by synchrotron radiation studies (see below).

To provide guidance for future faceting studies of planar surfaces, we have been collaborating with the group of R. Blaszczyszyn to conduct field-emission microscopy studies (15). In this work, a nearly hemispherical emitter tip, coated with metallic overlayers, develops facets on annealing. The typical

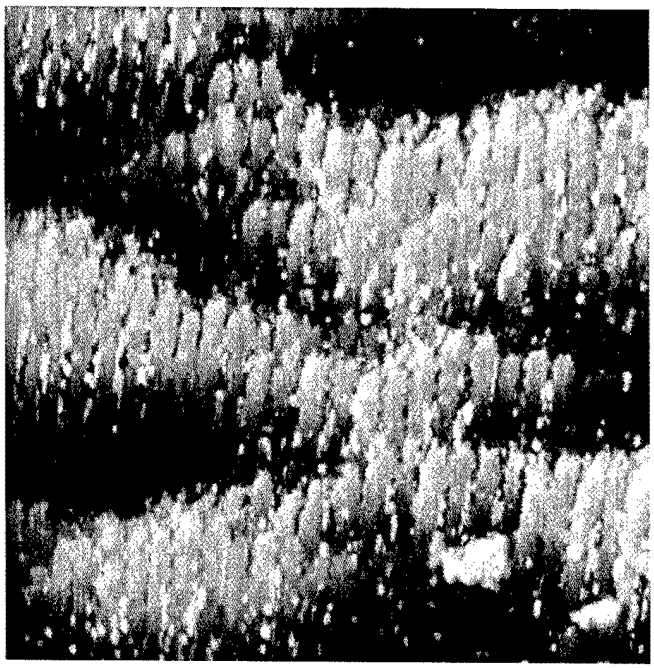

Fig. 3. STM scan ≈0.8 ML of Pd on W(211), annealed at 1000 K (1,000 Å × 1,000 Å). Dark vertical lines are identified as missing rows of Pd atoms; bright spots decorating the missing rows are attributed to adsorbed background gases. The average separation between missing rows is ≈50 Å, consistent with the ≈ (11 × 1) superstructure seen using LEED. [Reproduced with permission from ref. 14 (Copyright 2001, Am. Chem. Soc.).]

emitter has a diameter of ≈200 nm; the shape and dimensions are a good approximation to a single catalyst particle, although a bit larger. Recent studies have focused on ultrathin films of Pt on W, Pt on Ir, and Pd on Mo (16). In general, on annealing the metal film-covered emitter tip, the shape changes from nearly hemispherical to more polyhedral. The faceting effect, i.e., growth of facets, is particularly pronounced for the Pt/W and Pd/Mo systems, and less so for Pt/Ir [consistent with the fact that we have not yet found evidence for metal-induced faceting of planar Ir(210); see below]. The facets that form on bcc W and Mo are {112}, {123} and {178}, whereas {116} and {115} grow on fcc Ir.

Surface Chemistry of Bimetallic Pd/W. The surface chemistry of small hydrocarbons on transition metal surfaces is relevant to many important catalytic processes. We focus here on acetylene chemistry, for which reaction pathways are known to be sensitive to surface structure (ref. 17; for a review see ref. 18). Acetylene cyclization, $3C_2H_2 \rightarrow C_6H_6$, is catalyzed by palladium and has been studied extensively on clean and modified surfaces, under ultrahigh vacuum as well as high-pressure conditions. Acetylene cyclization is extremely structure-sensitive, so it is an ideal reaction for probing the effects of surface electronic and geometric structure. Isotopic studies indicate that benzene forms from acetylene in a stepwise fashion on Pd(111) and Cu(110); the reaction proceeds via a C_4 intermediate species, and the reactants do not undergo C—C or C—H bond scission (17–19).

Bimetallic systems can improve both activity and selectivity. For example, we have shown in a combination high-resolution electron-energy-loss-spectroscopy (HREELS) and TPD study that a single ML of Pd on W(211) decreases the high reactivity of W for C_2H_2 decomposition, and catalyzes self-hydrogenation of C_2H_2 to C_2H_4 and cyclization of C_2H_2 to C_6H_6 (20). Evidence for finite size effects in benzene formation has been reported by Goodman *et al.* (21) for Pd clusters supported on alumina films; Lambert *et al.* (22) have shown that there is a minimum ensemble on Pd(111) (≈7 atoms) necessary for benzene formation. Although it is clear that electronic structure plays an important role in the cyclization reaction, these studies suggest questions: can electronic structure alone be responsible for these known size effects? What are the effects of geometrical parameters, e.g., size and shape?

Zhdanov and Kasemo (3) have recently performed Monte Carlo analyses on the model catalytic reaction $2A + 2B \rightarrow 2AB$, which indicate that the reaction kinetics on a faceted nanocrystal can be different from those on a single crystal surface. The simulations have identified a kinetic "structure gap" not associated with special electronic effects or properties of small particles, but with their size and shape. They argue that geometric structure alone can play an important role in reaction kinetics. It is this idea that we are testing.

We have found that acetylene reactions over Pd/W(111) surfaces exhibit size effects on the nanometer scale (23). In these studies, we have characterized the self-hydrogenation of C_2H_2 to form C_2H_4 and cyclization of C_2H_2 to form C_6H_6 on planar and faceted Pd-covered W(111) and on Pd-covered W(112). The substrates ranged from 1 ML of Pd on planar W(211), to faceted Pd/W(111) surfaces containing different facet-size distributions. The goal is to probe the influence of facet size on reactivity. Below ≈700 K annealing temperature, the Pd/W(111) surface remains planar. Above ≈700 K, Pd-covered W(112) facets are formed, which grow in size with increasing annealing temperature. We have measured TPD spectra for self-hydrogenation of adsorbed C_2H_2 to form C_2H_4 product (Fig. 4). The ethylene TPD spectra for Pd/W(111) evolve in a systematic fashion as the surface is thermally converted into a faceted substrate, and the facets grow in size. For the largest facets (annealing T ≈ 1,000 K), the ethylene TPD spectrum is similar to that for C_2H_4 formation over planar Pd/W(112) (Fig. 4 *Upper*). Similar facet-size effects are seen for acetylene cyclization to form benzene (Fig. 4 *Lower*). The data provide clear evidence that size effects at the nanometer scale (3) should be considered in evaluation of reactivity data for faceted bimetallic surfaces.

Synchrotron Radiation Studies of Metals on W. During the last several years, we have found that certain ultrathin films (≈1 physical ML) on W(111) and Mo(111) substrates can induce faceting (e.g., Rh, Pd, Ir, Pt, Au, as well as O, Cl), whereas others do not [e.g., Ti, Co, Ni, Cu, Ag, Gd (10, 11)]. We noted a correlation, namely, that the elements that cause faceting have Pauling electronegativity >2.0, whereas the elements that do not cause faceting have electronegativities <2.0; W and Mo each have negativity = 1.7. This observation suggested that electronic structure plays a role in faceting. To search experimentally for possible electronic factors that influence faceting, we use HRSXPS based on synchrotron radiation. We study (mainly) the sharp W 4f, Pt 4f, Ir 4f, etc., and measure surface core level shifts (SCLS). Based on an extensive set of measurements, we can draw a number of conclusions.

(*i*) Although the SCLS is an extremely sensitive and useful indicator of interface formation, there is no clear correlation between Pauling electronegativity and surface or interfacial $4f_{7/2}$ binding energies (24). This finding was not unexpected, because the Pauling electronegativity is a measure of initial-state charge transfer effects, whereas the measured 4f-binding energies are influenced by a combination of initial and final-state effects.

(*ii*) Metals with the highest heats of adsorption (e.g., Pt, Pd), and the highest W4f interfacial binding energies are those which cause faceting (24). This finding is consistent with a first-principles theory that indicates that a higher heat of adsorption provides both a strong thermodynamic driving force for faceting and a lower kinetic barrier to faceting (25, 26).

(*iii*) For most systems studied [Cu, Ni, Rh, Pd, Ir, Pt, Au on

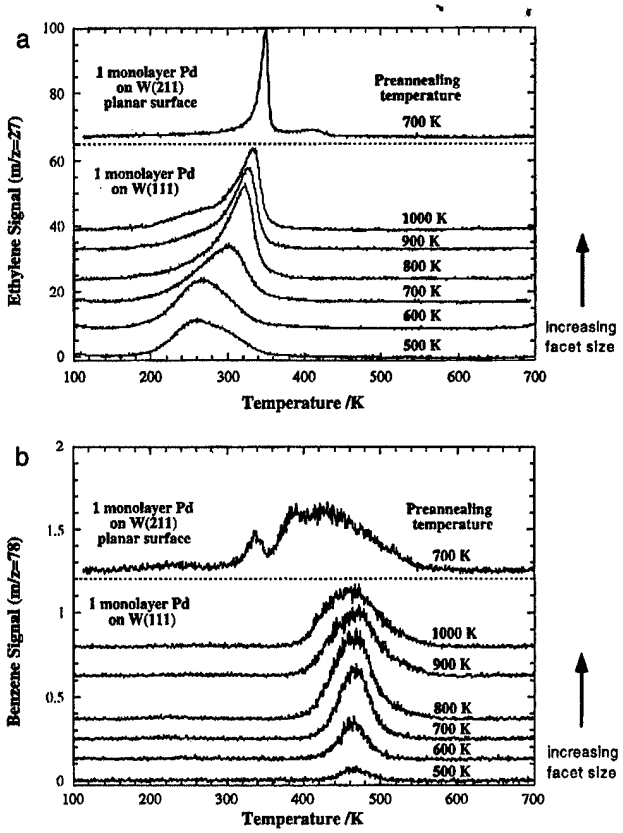

Fig. 4. (*a* and *b*) Surface chemistry of acetylene on planar and faceted Pd/W surfaces. (*Top*) TPD spectra for C_2H_4 reactively formed after adsorption of a saturation coverage of C_2H_2 at 100 K onto Pd-covered W (C_2H_2 exposure $\approx 3 \times 10^{-6}$ torr·s). In each case, the metal is precovered with 1 ML of Pd and annealed to the indicated temperature, before deposition of C_2H_2. The sizes of {211} facets increase with annealing temperature >700 K. (*Bottom*) TPD spectra for C_6H_6 reactively formed after adsorption of C_2H_2 on Pd/W surfaces, as in *a*.

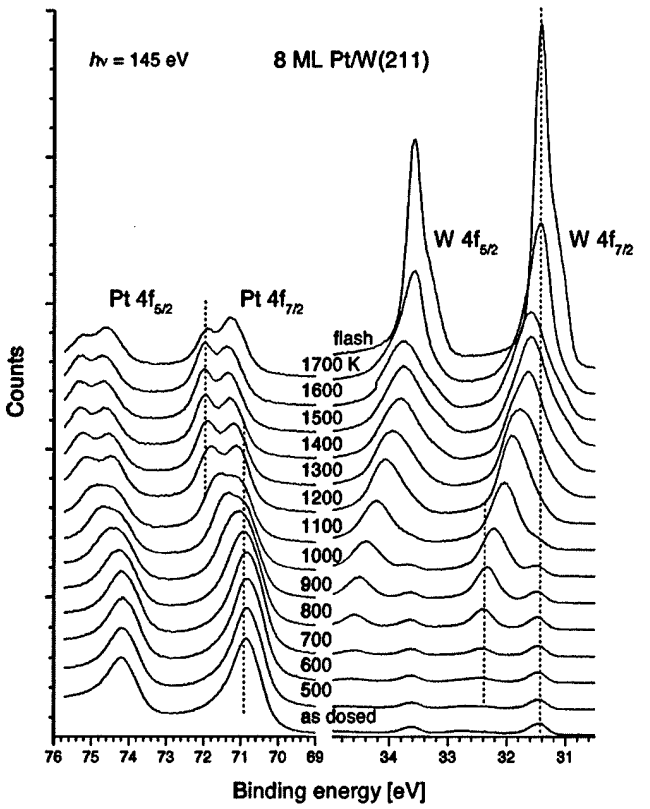

Fig. 5. Evidence for formation of interfacial alloy in Pt 4f and W 4f SXPS spectra associated with an annealing sequence for an 8 ML Pt film on W(211). Annealing time is 1 min at each temperature. Features on high binding energy sides of each 4f peak indicate that W atoms diffuse through the interface to form a Pt-W alloy film. [Reproduced with permission from ref. 28 (Copyright 2000, Am. Phys. Soc.)]

W(111) and W(112); refs. 27–29], we find evidence that a 1 ML of overlayer metal is thermally stable, and floats on the outer surface without significant alloy formation, for all temperatures up to the onset of desorption. For all systems except Au/W, we find that multilayer films form alloys on annealing: invariably, W atoms from the substrate diffuse into the overlayer film, rather than vice versa. In certain cases (Pt/W, Ir/W) we can measure sharp 4f levels of both overlayer and substrate, and find evidence for alloy formation in multilayer films (Fig. 5). In general, the alloying behavior of the bimetallic systems investigated here is consistent with the known bulk-phase diagrams (e.g., Pt is not soluble in W, but W is soluble in Pt to a maximum of ≈60% W). Moreover, we have used Born–Haber cycles and the equivalent core approximation to extract thermochemical data concerning energetics of adhesion, segregation and alloying in these systems (28).

(*iv*) We find evidence for intermixing at the interface for multilayer deposition of several metals (Pt, Ir, Rh) on W(111) at room temperature (29)! This finding is surprising to those in the thin film community (e.g., for those studying magnetic thin films) who generally believe that thin films of high-melting-temperature materials form abrupt interfaces.

Faceting and Surface Chemistry of Ir(210). As part of a larger effort to study the morphological stability of adsorbate covered metallic surfaces, we have investigated the influence of various adsorbates on fcc Ir(210). The structure of the atomically rough Ir(210) surface is similar to that of bcc W(111), but with reduced symmetry (2-fold). Based on studies using LEED and STM, we find that oxygen overlayers induce substantial facets on Ir(210), whereas the metal overlayer studied to date (Au) does not cause faceting.

When Ir(210) is exposed to more than ≈0.9 L (1 L = 1×10^{-6} torr·s; 1 torr = 133 Pa) of oxygen and annealed to $T > 600$ K, it experiences significant morphological restructuring: nanometer-scale pyramid-like structures (facets) are formed on the initially planar surface (I.E., K.P., and T.E.M., unpublished data.). LEED measurements show that the pyramids have three sides with mirror symmetry (two {311} facets and one {110} facet), and that the faceted surface exhibits a quasi-reversible behavior on annealing to higher temperatures. The surface reverts to its planar state at temperatures above 850 K but, provided the maximum annealing temperature is below the desorption temperature of oxygen, facets reappear on cooling to temperatures below 800 K. Furthermore, we are able to remove the oxygen from the surface by means of catalytic oxidation of CO at ≤580 K or by means of the H_2 + O reaction at ≤400 K, while preserving the faceted structure. TPD and Auger electron spectroscopy have shown that residual adsorbed O and CO (or H) are negligible after this procedure. The faceted clean surface is stable up to 600 K, but irreversibly reverts to the planar state above 600 K. These experiments indicate that the clean, faceted, metastable Ir(210) surface provides an ideal substrate to study thermal relaxation of nanometer-scale surface features.

In a previous section we reported that C_2H_2 reacts on planar and faceted Pd/W to form C_2H_4 and C_6H_6 products. In contrast, the clean Ir(210) surface is considerably more aggressive in

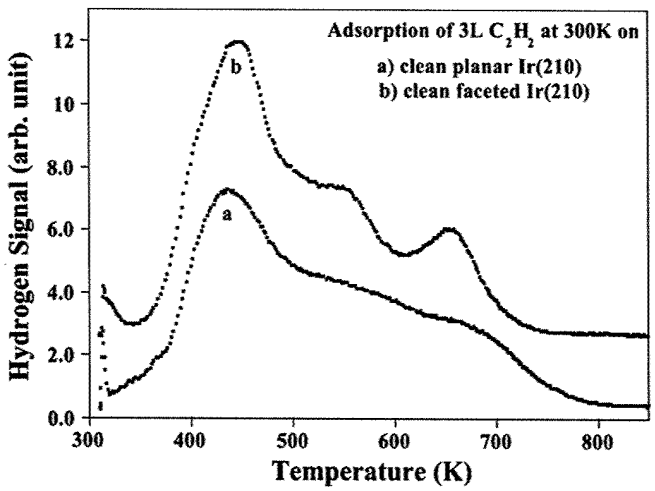

Fig. 6. TPD spectra for H_2 reactively formed after adsorption of a saturation coverage of C_2H_2 onto planar Ir(210) (curve a) and onto the clean, faceted Ir(210) surface (curve b). In each case, the C_2H_2 dose is $\approx 3 \times 10^{-6}$ torr·s (3 L) onto the substrate at 300 K. The differences in the TPD spectra illustrate the structure-sensitivity of C_2H_2 surface chemistry.

dissociating C_2H_2 than the Pd/W surfaces. We find that adsorption of C_2H_2 on Ir(210) at either 100 K or 300 K leads to dissociation when the surface is heated, and that the dominant desorption product (>99%) in TPD spectra is H_2. Traces of C_2H_4 are seen at low temperature in TPD.

TPD spectra for desorption of H_2 from hydrogen-dosed Ir(210), and desorption of H_2 from acetylene-dosed Ir(210) exhibit differences that indicate clearly that desorption of H_2 from C_2H_2-dosed Ir is reaction-rate limited (W.C., I.E., Q.W., and T.E.M., unpublished data). This reactivity is almost certainly caused by formation of intermediate fragments (30, 31) that may dissociate in a stepwise fashion on heating ($-CCH$? $-CCH_3$?).

Fig. 6 provides vivid evidence for structure sensitivity in C_2H_2 decomposition over Ir surfaces. Here, we compare TPD spectra of H_2 after C_2H_2 deposition on clean planar Ir(210) and on clean faceted Ir(210); the clean faceted surface was prepared as described above. There are striking differences in the TPD spectra that arise from the nanoscale surface structure on the faceted surface. We are using HREELS and HRSXPS in an attempt to identify the stoichiometry and concentration of the intermediates on the planar and faceted surfaces.

Nucleation of Nanoscale Clusters of Cu on S(4 × 4) W(111). Studies of sulfided surfaces of W may have interesting implications for hydrodesulfurization (HDS) catalysis, a process of great importance for removing S-impurities from petrochemicals. The HDS process is typically catalyzed by Mo or W sulfides that are promoted with group VIII transition metals.

In earlier studies of the sulfided W(111) surface, we found that S induces an unusual reconstruction with (4 × 4) periodicity (32). The sulfur-covered W(111) surface (S(4 × 4)/W(111) is characterized by broad, planar terraces ≈30 nm in width. We recognized the possibility that this highly corrugated sulfided surface might offer the opportunity for site-dependent nucleation of metal nanoclusters; such arrays of nanoclusters may, in turn, have unusual chemical properties.

We have now studied the interactions of vapor-deposited Cu with the highly ordered S(4 × 4)/W(111) surface, by means of STM, LEED, and Auger electron spectroscopy (33). We found that fractional monolayers of Cu grow homogeneously as clusters on S(4 × 4)/W(111) over a wide Cu coverage range. At low Cu coverages (<0.1 ML), Cu nanoclusters are found to nucleate preferentially at characteristic 3-fold hollow sites on the sulfided surface; there is a clear energetic preference for one type of site over others (Fig. 7). The formed Cu nanoclusters are uniform in size as coverage increases, indicating self-limiting growth (the clusters are ≈0.5 nm in diameter, and contain ≈3 atoms). The self-limiting growth may be attributed to a repulsive interaction between diffusing Cu atoms and stable nanoclusters arising from lattice mismatch between the Cu metal and the sulfided substrate. As Cu coverage increases ≥0.1 ML), cluster formation and growth occur without limitation on other adsorption sites (atop and vacancy).

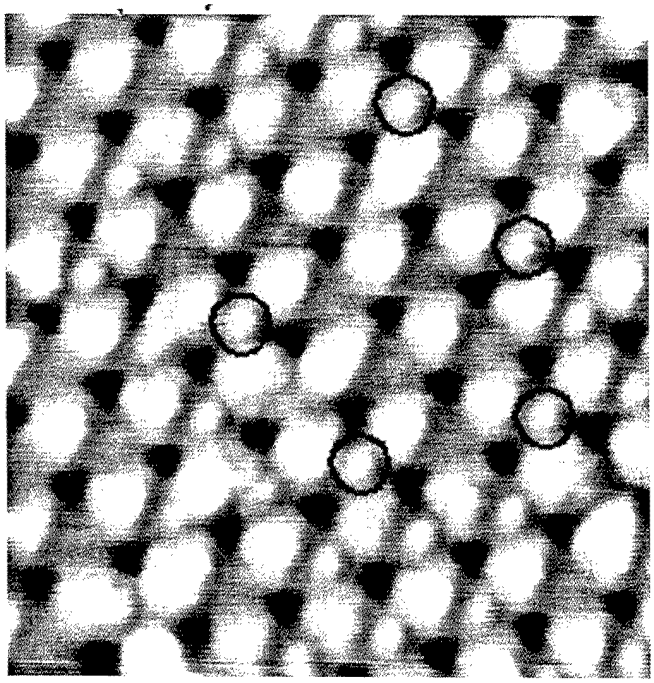

Fig. 7. STM image (100 Å × 100 Å) of 0.05 ML of Cu on S(4 × 4)/W(111). Nanoclusters with uniform size are found to nucleate preferentially in characteristic 3-fold hollow sites. Nanoclusters are estimated to be ≈5 Å in diameter; a few examples are highlighted with circles in the image.

The observation of unusual growth for a metal on sulfided W(111) is an impetus for further studies of catalytically active metals (Co, Ni) that have direct relevance to the fundamentals of hydrodesulfurization catalysis.

Concluding Remarks. The main factor that distinguishes this work from other studies of model bimetallic and sulfide catalysts is our emphasis on atomically rough, high-surface-energy surfaces that may be morphologically unstable during reaction conditions. For example, the observation of faceting demonstrates that the surface is not a rigid template, but it may undergo massive structural rearrangements when covered by a metallic film under reaction conditions. The exposed surfaces may be quite different from those present in the absence of the overlayer metal. We believe that these results are important for understanding dynamic structural rearrangements at the surfaces of high area bimetallic and sulfide catalysts, and in clarifying the role of nanometer-scale size effects in surface reactions.

We acknowledge valuable discussions with and contributions of various collaborators, including R. Blaszczyszyn, J. G. Chen, C.-T. Chan, G. L. Kellogg, and J. B. Hannon. This work has been supported in part by the U. S. Department of Energy, Division of Chemical Sciences, and by U. S. Army Research Office, Durham, NC.

1. Valden, M., Lai, X. & Goodman, D. W. (1998) *Science* **281,** 1647–1650
2. Heiz, U., Sanchez. A., Abbet, S. & Schneider, W.-D. (1999) *J. Am. Chem. Soc.* **121,** 3214–3217.
3. Zhdanov V. P. & Kasemo, B. (1998) *Surf. Sci.* **405,** 27–37.
4. Sinfelt, J. H. (1983) *Bimetallic Catalysts* (Wiley, New York).
5. Anonymous (1982) *Advances in Multimetallic Catalysts* (Catalytica Associates, Inc., Santa Clara, CA).
6. Kuznetsov, B. N., Yermakov, Yu. I., Boudart, M. & Collman, J. P. (1978) *J. Mol. Catal.* **4,** 49–57.
7. Leclercq, C., Romero, S., Pietrzyk, T. S., Grimblot, J. & Leclercq, L. (1984) *J. Mol. Catal.* **25,** 67–86.
8. Yermakov, Yu. I., Kuznetsov, B. N. & Ryndin, Yu. A. (1976) *J. Catal.* **42,** 73–78.
9. Trunschke, A., Ewald, H., Gutschick, D., Miessner, H., Skupin, M., Walther, B. & Böttcher, H.-C. (1989) *J. Mol. Catal.* **56,** 95–106.
10. Madey, T. E., Guan, J., Nien, C.-H, Tao, H.-S., Dong, C.-Z. & Campbell, R. A. (1996) *Surf. Rev. Lett.* **3,** 1315–1328.
11. Madey, T. E., Nien, C.-H., Pelhos, K., Kolodziej, J. J., Abdelrehim, I. M. & Tao, H.-S. (1999) *Surf. Sci.* **438,** 191–206.
12. Pelhos, K., Hannon, J. B., Kellogg, G. L. & Madey, T. E. (1999) *Surf. Sci.* **432,** 115–124.
13. Pelhos, K., Madey, T. E., Hannon, J. B. & Kellogg, G. L. (1999) *Surf. Rev. Lett.* **6,** 767–774.
14. Pelhos, K., Abdelrehim, I. M., Nien, C.- H. & Madey, T. E. (2001) *J. Phys. Chem. B* **105,** 3708–3717.
15. Pelhos, K., Madey, T. E. & Blaszczyszyn, R. (1999) *Surf. Sci.* **426,** 61–68.
16. Antczak, G., Madey, T. E., Blaszczyszyn, M. & Blaszczyszyn, R. (2001) *Vacuum* **63,** 43–51.
17. Omerod, R. M., Lambert, R. M., Bennett, D. W. & Tysoe, W. T. (1995) *Surf. Sci.* **330,** 1–10.
18. Abdelrehim, I. M., Pelhos, K., Eng J., Jr., Chen, J. G. & Madey, T. E. (1998) *J. Mol. Catal. A* **131,** 107–120.
19. Lambert, R. M. & Ormerod, R. M., (1994) in *Surface Reactions*, Springer Series in Surface Science, ed. Madix, R. J. (Springer, Berlin), Vol. 34, pp. 89–134.
20. Abdelrehim, I. M., Pelhos, K., Madey, T. E., Eng, J., Jr. & Chen, J. G. (1998) *J. Phys. Chem. B* **102,** 9697–9707.
21. Holmblad, P. M., Rainev, D. R. & Goodman, D. W. (1997) *J. Phys. Chem. B* **101,** 8883–8886.
22. Baddeley, C. J., Tikhov, M., Hardacre, C., Lomas, J. R., Lambert, R. M. (1996) *J. Phys. Chem.* **100,** 2189–2194.
23. Barnes, R. Abdelrehim, I. M. & Madey, T. E. (2001) *Topics Catal.* **14,** 53–61.
24. Tao, H.- S., Rowe, J. E. & Madey, T. E. (1998) *Surf. Sci.* **407,** L640–L646.
25. Che, J. G., Chan, C. T., Kuo, C. H. & Leung, T. C. (1997) *Phys. Rev. Lett.* **79,** 4230–4233.
26. Nien, C.-H., Madey, T. E., Tai, Y. W., Leung, T. E., Che, J. G. & Chan, C. T. (1999) *Phys. Rev. B* **59,** 10335–10340.
27. Kolodziej, J. J., Pelhos, K., Abdelrehim, I. M., Keister, J., Rowe, J. E. & Madey, T. E. (1999) *Prog. Surf. Sci.* **59,** 117–134.
28. Kolodziej, J. J., Madey, T. E., Keister, J. W. & Rowe, J. E. (2000) *Phys. Rev. B* **62,** 5150–5162.
29. Kolodziej, J. J., Madey, T. E., Keister, J. W. & Rowe, J. E. (2002) *Phys. Rev. B,* in press.
30. Eng, J., Jr., Chen, J. G., Abdelrehim, I. M., Madey, T. E. (1998) *J. Phys. Chem B* **102,** 9687–9696.
31. Marinova, Ts. S., & Kostov, K. L. (1987) *Surf. Sci.* **181,** 573–585.
32. Nien, C.-H., Abdelrehim, I. M. & Madey, T. E. (1999) *Surf. Rev. Lett.* **6,** 77–96.
33. Wu, Q., Chen, W. & Madey, T. E. (2002) *J. Phys. Chem.*, in press.